2018

Catalytic Oxidation of Methane Over Alumina Supported Palladium Oxides

Jacqueline Michelle McGuire

Follow this and additional works at: https://csuepress.columbusstate.edu/theses_dissertations

Part of the Chemistry Commons

Recommended Citation

CATALYTIC OXIDATION OF METHANE OVER ALUMINA SUPPORTED PALLADIUM OXIDES

Jacqueline Michelle McGuire

COLUMBUS STATE UNIVERSITY

CATALYTIC OXIDATION OF METHANE OVER ALUMINA SUPPORTED PALLADIUM

OXIDES

A THESIS SUBMITTED TO

THE COLLEGE OF LETTERS AND SCIENCES

IN THE PARTIAL FULFILLMENT OF

THE REQUIREMENTS FOR THE DEGREE OF

MASTER OF SCIENCE

DEPARTMENT OF CHEMISTRY

BY

JACQUELINE MICHELLE MCGUIRE

COLUMBUS, GEORGIA

2018

CATALYTIC OXIDATION OF METHANE OVER ALUMINA SUPPORTED PALLADIUM

OXIDES

By

Jacqueline Michelle McGuire

Committee Chair:

Dr. Anil C. Banerjee

Committee Members:

Dr. Zewdu Gebeyehu
Dr. Daniel Wade Holley

Columbus State University
May 2018

ABSTRACT

The objectives of this research include development and characterization of alumina supported palladium oxide catalysts for low temperature catalytic oxidation of methane. The catalysts were prepared by various methods and then characterized and screened to select the best catalyst for further studies. A 5% (wt/wt) Pd/γ-Al_2O_3 catalyst prepared by an improved vortex-assisted incipient wetness method showed the best activity of 94% (mol/mol) methane conversion at 325 °C. The active surface species was found to be PdO and Pd native oxides (PdNtv) as confirmed by X-ray Photoelectron Spectroscopy and activity studies. The γ-Al_2O_3 support played an integral role in the formation of Pd native oxides as well as a facilitator in oxygen mobility.

INDEX WORDS: Supported Palladium Catalysts, Palladium Oxide, Palladium Native Oxide, Aluminum Oxide, Methane Oxidation, Methane Combustion

To

Micah,

Lilli, Ezra and Trace

Thank you for sacrificing so much and allowing me to pursue what I love.

You're my biggest fans.

ACKNOWLEDGEMENTS

TABLE OF CONTENTS

LIST OF TABLES

LIST OF FIGURES

I. Introduction and Background Information

A.   **Introduction**

Methane is the second most prevalent greenhouse gas behind carbon dioxide with a global warming potential 25 times more.[1] While there are a variety of naturally occurring sources that contribute significantly to the overall contribution of methane to the atmosphere, there are many anthropogenic sources which hold a special focus to researchers because the contribution from these sources can be mitigated. Within the U.S. in recent years, political conflict has led to legislation (i.e. the President's *Climate Action Plan: Strategy to Reduce Methane Emissions*) aimed at moderating emission of greenhouse gases including methane.[2-3] Most recently, courts ruled in favor of regulations that restrict any emissions of methane from natural gas wells on federal land. The solution to most recent legislation is the burning of that emitted methane.[4] An agenda to control emissions has encouraged researchers to develop innovative techniques to lessen methane in the atmosphere. One technique involves use of catalysts to convert methane into a less harmful or shorter-lived species. Of these catalysts, palladium shows promise for conversion of methane at low-temperatures, lending hope to automakers and industries using turbines powered by natural gas.[5] The development of improved catalysts entails understanding the mechanism of the surface reaction taking place in the conversion of one gas to another, as well as the constituents of the species involved.

B.   **Atmospheric Methane**

Methane is a highly flammable, colorless, odorless gas with a melting point of -183 °C and a boiling point of -161°C. At 20 °C, its solubility in water is 3.3ml per 100ml of water. It is lighter than air with a relative density of 0.6 (air = 1). Its auto ignition temperature is 537 °C, and its explosive limits are 5-15 vol% in air.[6] It is listed among the top 5 greenhouse gases.

Greenhouse gases warm the Earth by trapping infrared radiation. This occurs either by directly absorbing radiation or through indirect radiative forcing when chemical reactions with one greenhouse gas (i.e., methane) produce other gases. Newly produced gases subsequently absorb radiation or disrupt other atmospheric gases and/or processes.[1] Of the top greenhouse gases, methane is second behind carbon dioxide, followed by nitrous oxide and fluorine-containing halogenated substances.

2015 Greenhouse Gases by Emissions
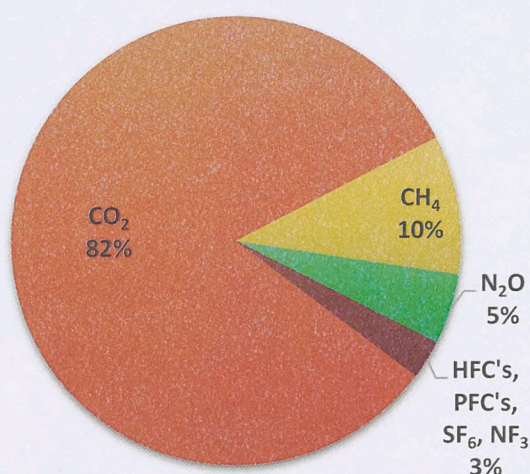
2015 Top Methane Sources

CO$_2$ 82%

CH$_4$ 10%

N$_2$O 5%

HFC's, PFC's, SF$_6$, NF$_3$ 3%

Petroleum Systems 6.1%

Other 16.0%

Enteric Fermentation 25.4%

Manure Management 10.1%

Landfills 17.6%

Natural Gas Systems 24.8%
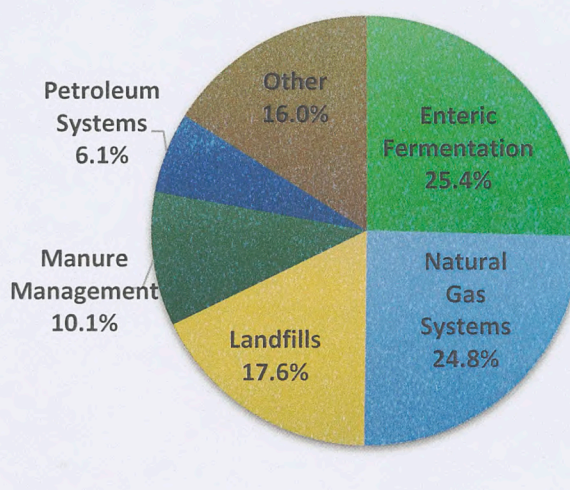
Fig. 1.1: Top Greenhouse Gases and Top Anthropogenic Methane Sources[1]

In 2015 methane made up 10% of all U.S. anthropogenic greenhouse gas emissions[1] and 15% globally.[7] Its global warming potential (GWP) is 25 times greater than CO$_2$ over a 100-year period,[1] however, in the short term it poses a much higher threat with a GWP of 72, if considered over a 20-year period. In the short term, methane accounts for 35% of global greenhouse emissions,[7] according to the monitoring methods currently used by the EPA. Critics of the EPA's "bottom-up" method claim that the actual methane emissions could be double the EPA's estimates.[8]

C.   Methane and the Automotive Industry

Use of natural gas is considered to be a possible transition between carbon intensive fossil fuels and renewable energy systems. It has an advantage over coal and petroleum in that it releases approximately half of the CO_2 emissions. However, there are methane leaks in the use of natural gas. Even leaks of only 1-5% could negate its green benefits because of methane's own high GWP value.[9] While methane was once ignored in clean air legislation, growing knowledge of its impact recently inspired closer inspection. A 2010 EPA report found that light-duty vehicles were responsible for 60% of all mobile greenhouse gas emissions. As a result, vehicles of year models 2017-2025 have been given new standards to regulate greenhouse gas emissions, including methane.[10] The rise of such regulations presents a critical need for methane-oxidation catalysts that help reduce emissions and improve performance. Currently employed catalysts are inefficient at reducing methane in exhaust streams. In addition, high temperature combustion leads to emissions of other undesirable gases like NO_x and CO. However, methane combustion assisted by heterogeneous catalysts could yield two beneficial outcomes in the form of lowering combustion temperatures to increase performance, while also limiting emissions.[11] Low-temperature methane combustion would also be of benefit in catalyst-assisted combustion within gas turbines fueled with natural gas. While the idea of low-temperature combustion is advantageous, finding a catalyst that can perform in such "lean-burn" conditions has been a challenge and little progress has been made over the course of 40 years of research.[5] Catalysts used for lean-burn conditions would need to overcome multiple obstacles, including: 1) operating at temperatures <500 °C and under low concentrations of methane (500-1000 ppm), 2) withstanding large amounts of water vapor, CO_2 and oxygen concentrations, and 3) tolerating presence of SO_x and NO_x. Two families of catalysts studied in more recent decades are noble metals and transition metal oxides. Both have shown

ability to completely oxidize methane, but the noble metals hold an advantage because they have superior specific activity. This makes them the best candidate for hydrocarbon combustion, especially in the case of methane which is the most difficult to activate. Of the noble metals Pt and Pd are the most commonly studied, however supported palladium catalysts have the best performance under lean-burn conditions.[12] Disputes exist over the most active phase of palladium as metallic Pd, palladium oxide (PdO), and non-stoichiometric Pd_xO_y have been identified in research as having catalytic activity.[13-15]

D.   Palladium and Palladium (II) Oxides

Palladium is a rare metal that is typically found in deposits of platinum, nickel, copper, silver, and gold. It is a silver, white, soft metal with a high resistance to corrosion, a quality which makes it ideal for electronic industries and dental alloys. It is widely used in the field of catalysis, from bulk production of nitric acid for fertilizers, to producing acetaldehyde as in the Wacker process, to reducing automobile exhaust emissions through heterogeneous catalysis.[16] Palladium has two main oxidation states, Pd(0) and Pd(II).[17] In its metallic state, palladium has a face-centered cubic structure as shown in Figure 1.2. The crystal structure of PdO is body-centered tetragonal, where each O ion is tetrahedrally coordinated to four Pd ions and each Pd ion is coordinated to four O ions in a square-planar orientation. The geometry of Pd in PdO is 4-coordinate, square planar as shown in Figure 1.3.[18]

Fig. 1.2: Face-centered Cubic Structure of Metallic Pd
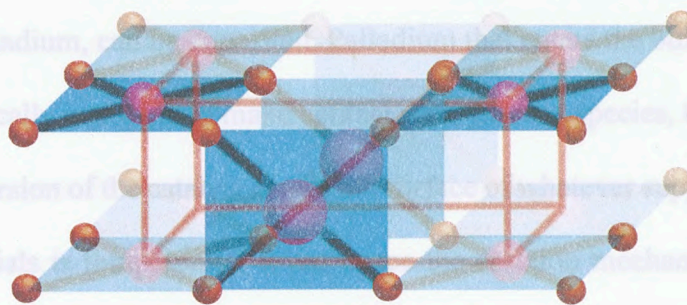
Fig. 1.3: Crystal Structure of PdO

In addition to metallic Pd and stoichiometric PdO, palladium oxide also exists as non-stoichiometric Pd_xO_y oxides also known as "native palladium oxide" (abbreviated as "PdNtv"). A native palladium oxide (PdNtv) is formed when palladium metal is exposed to the air for a few days. Most native oxides are not stoichiometric. A stoichiometric palladium oxide (PdO) is formed when a native palladium oxide is calcined. Due to its non-stoichiometric nature, native palladium oxide is often designated as PdO_x. The surface of a solid catalyst can be very different than the "bulk" (or interior), due to the greater reactivity. For example, the bulk of a catalyst could be micro-structured with PdO, while the surface composition exists as non-stoichiometric (or native) palladium oxide.[19]

E. Palladium for Low-Temperature Combustion of Methane

In regard to catalyzing methane, palladium has been the element of choice in recent years, even though the mechanism of its action is still not fully understood. What is known, however, is that palladium is the best performer at low temperatures which are typical of lean-burn conditions.[12] To date, an ideal catalyst that performs optimally under 300 °C is undiscovered, but palladium, supported on various materials comes close, as it has been shown to initiate oxidation at 400 °C.[5] The support can be alumina, silica, carbon, or any material with high melting points

and decomposition temperatures.[20] The role of the support is to provide an extensive surface area upon which the catalyst, in this case palladium, can be deposited. Palladium that enters the bulk is of no use catalytically, as it is not physically available to make contact with gaseous species, thus it is important to achieve thorough dispersion of the catalyst across the surface of whatever support is used. Another role of support materials is the potential to influence the reaction mechanism itself.[21] Some supports contain promoters, such as alkali metals or barium or lanthanum oxides, which can assist the catalyst in product desorption by donating electron density.[14, 15] These are important concepts in catalysis as they affect a catalyst's conversion and catalytic turn-over rates. Another consideration, is the possibility of the support to lend its constituents to the catalytic active site during the course of the reaction.[21, 22] For example, regarding aluminum oxide (Al_2O_3), under some situations, the oxygen from the aluminum oxide could migrate to the palladium, forming PdO or some form of PdO_x and/or migrate to the gas-phase molecule providing oxygen for the combustion.[23] This mechanism is under-explored and is one that this research seeks to advance evidence to support or reject.

Aluminum oxide (alumina) is a favorable support for the combustion of methane. It is available in nature in bauxite and corundum,[24] and can be made in the laboratory by the Bayer process.[25] Alumina is favorable because its surface area and structural features create differing shapes of support. Independent studies have reported on the benefits of alumina for the combustion of methane.[12, 21, 23, 26-27] Alumina comes in many forms and particle sizes. Of interest to catalysis are the α- and γ-alumina nanopowders. α-Alumina is the most stable form,[28-29] but γ-alumina is sufficiently porous, thus a preferred support for palladium.[30-31] The structure of γ-alumina is traditionally considered a cubic defect, in which the oxygen atoms are closely cubic packed and the aluminum atoms occupy octahedral and tetrahedral sites.[31]

Several methods exist for preparing a catalyst so that active sites are evenly dispersed on the surface.[20, 27] Of those methods, three are explored in the course of this research: incipient wetness, wet impregnation, and slurry. Incipient wetness method utilizes the capillary action of the pores in the dry alumina to draw in a precursor solution which is slowly added to the support and palladium gets dispersed across the surface of the alumina. Wet impregnation uses the same capillary action concept, but in the reverse, where the dry alumina is added to the palladium solution. With the slurry method, both support and precursor are combined in a liquid phase. All three methods require extensive mixing for sufficient dispersion.[14]

Catalyst precursors are stable, solid or salt forms of the metal catalyst. The precursors themselves do not make for good catalysts, but they assist in precursor solubility so that the metal can be added to a support.[20] To obtain the final active catalyst, the precursor and support mixture must go through a process of calcination. This process heats the dry precursor/support mixture up above the temperature of decomposition of any nitrate/carbonate components and helps form metal-oxide links with the support.[14] All water and undesired compounds are removed, and remaining, are the final active catalytic sites on support material. In the case of the palladium precursor, $Pd(NO_3)_2 \cdot xH_2O$, the nitrate and water are decomposed during calcination to result in Pd and/or PdO on the support. The temperature at which the calcination takes place must be carefully determined. If the temperature is not high enough, the necessary decomposition will not take place. If the temperature is too high, sintering is a risk when metallic particles, without melting, cohere together in larger particle sizes thus ruining ideal dispersion and greatly decreasing catalytic surface area. The temperature of calcination also effects the formation of metal oxides. In a review of noble metal catalysts, Gélin and Primet describe numerous preparations and calcination temperatures, reporting a trend among researchers where lower calcination

temperatures favor PdO formation and higher temperatures tend to form more metallic palladium.[12] Several different calcination temperatures were explored in this research.

F.   Kinetics and Surface Reactions

Even after a catalyst is determined which can catalyze within the optimal temperature range, to further develop it or improve reaction conditions, the mechanism of the surface reaction must be understood. The catalytic cycle might be described as a "black box," but kinetics studies provide a glimpse inside that box that lend helpful mechanistic assumptions. Monitoring the kinetics of the reaction or the concentration of reactant, intermediates, and/or products, over time, can provide information regarding the mechanism, catalytic activity, and product selectivity. Several instruments can help with this (ex. gas chromatography, mass spectrometry), however this research utilizes gas chromatography (GC) to monitor the changing methane and carbon dioxide concentrations over time. Plotting the change in concentration over time yields a reaction profile that can facilitate formulation of a reaction mechanism that agrees with the experimental observations, often revealing a rate-determining step. Once a rate is determined, one can infer a reaction order, rate law and calculate a rate constant. Langmuir-Hinshelwood (L-H) kinetics provide an example model to describe common heterogeneous catalytic reactions following bimolecular surface reaction (Figure 1.4). This model assumes the gas phase reactants must first adsorb to catalytic active sites on the surface of the solid support. The reaction then takes place on the surface, followed by product desorption back to the gaseous phase.[14]
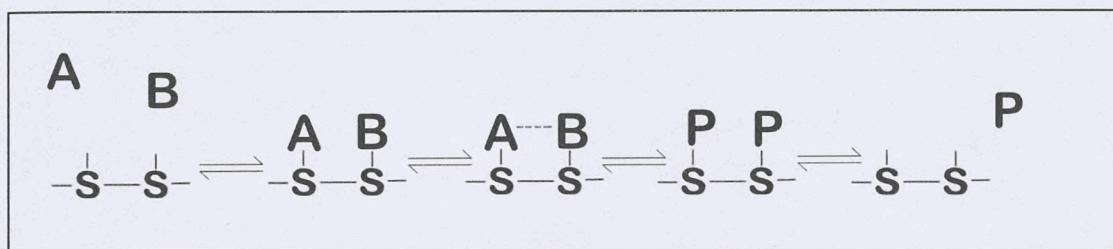
Fig. 1.4: Langmuir-Hinshelwood Mechanism

The reaction can be described as $A + B \xrightarrow{catalyst} P$, and the rate as: $r = k[A]^\alpha [B]^\beta$, where α and β indicate the order of the reaction. But the L-H model is highly dependent on sites available versus sites occupied, thus introducing two new characters: θ_A and θ_B, where θ_A represents the fraction of sites occupied by A, and θ_B likewise represents sites occupied by B. This means that the only available sites are those represented by: $1 - \theta_A - \theta_B$, thus providing the following rates at equilibrium where $r_a = r_d$:

a) rate of adsorption of A: $r_{a_A} = k_a p_A (1 - \theta_A - \theta_B)$, where p refers to partial pressure (or conc.);

b) rate of adsorption of B: $r_{a_B} = k_a p_B (1 - \theta_A - \theta_B)$;

c) rate of desorption of A: $r_{d_A} = k_d \theta_A$; and

d) rate of desorption of B: $r_{d_B} = k_d \theta_B$.

If a new constant, K, is introduced to represent $\frac{k_a}{k_d}$, then by algebraically combining rate conditions for A and B, we eventually arrive at the following L-H rate law (Atkins):

$$r = k_2 \theta_A \theta_B = \frac{k_2 K_A p_A K_B p_B}{(1 + K_A p_A + K_B p_B)^2}$$

While the L-H mechanism is much more common in heterogeneous catalysis, another type of mechanism to consider is the Eley-Rideal mechanism. In this model, one gas phase reactant, A,

adsorbs on the surface of the catalyst and the gas-phase reactant, B, interacts with A independent of the catalyst surface, to form product P.
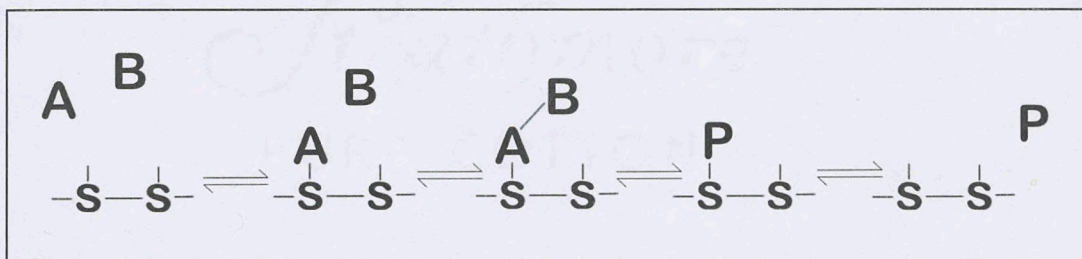
Fig. 1.5: Eley-Rideal Mechanism

In this mechanism where $A + B \xrightarrow{catalyst} P$, the rate of formation is expected to be proportional to the partial pressure of B, p_B, and the surface coverage is only represented by θ_A, therefore the rate law in this case should be: $r = k_2 p_B \theta_A$, where $\theta_A = \frac{Kp_A}{1+Kp_A}$. Therefore, the overall rate law according to Eley-Rideal is:

$$r = \frac{k_2 Kp_A p_B}{1 + Kp_A}$$

To complicate simple adsorption and desorption, factors in the catalytic cycle can decrease turnover number, which is the number of cycles before the catalyst deactivates. If a reactant does not adsorb strongly enough, the reaction may never occur. If a reactant or product adsorbs too strongly, available active sites will decrease, and the catalyst may be deactivated. These concepts are the basis behind Sabatier's principle and can be illustrated in a volcano plot, which is a graphical representation of reaction rate versus heat of adsorption (Figure 1.6).
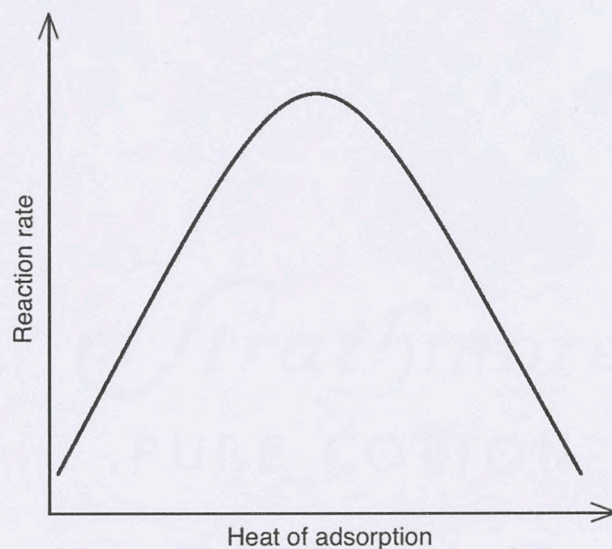
Fig. 1.6: Volcano Plot

Besides the heat factor, the life of a catalyst can come to an end via deactivation, sintering, inhibition, or poisoning. Deactivation describes a circumstance in which a catalyst becomes less active, deviating from its ideal rate law. This deviation can also follow its own first or second-order rate law. A catalyst can be deactivated when products, by-products, or other compounds present in the gas mixture occupy active sites, lowering conversion rates. In an extreme case, the catalyst could be poisoned, in which the active sites are occupied irreversibly and thus destroyed. Active sites can also be destroyed by sintering, a type of thermal degradation in which high temperature cause either support pore collapse or the size of metal crystallites to change. Both processes result in loss of surface area. As a general rule, a metal will begin to sinter when the temperature is at roughly half of the metal's melting point.[14] These important factors must be considered when designing the catalyst and studying its kinetics.

G.   Objectives of this Study

This research aimed to achieve three specific objectives toward the advancement in catalyzed low-temperature combustion of methane. Firstly, it sought to identify a supported palladium catalyst that is suitable for complete combustion of methane below 400 °C, and a specific preparation method to develop such a catalyst. Secondly, this research sought to characterize the surface composition of both fresh and used catalysts, to aid in understanding potential surface reactions. Lastly, this research attempted to contribute on the kinetics and mechanism of the surface reactions in the catalytic oxidation of methane over supported palladium catalysts.

In pursuit of the first objective, a palladium catalyst was sought through several preparations that displayed catalytic activity with over 80% methane conversion rates at temperatures <400 °C. In 2001, Gélin and Primet conducted a comprehensive review of Pt and Pd supported catalysts, many of which were using alumina supports.[12] Over a decade later, recent literature continues to confirm aluminum oxide as an optimal support for palladium. Miller et. al conducted a study on the support effects where Pd is used for methane oxidation. In this study where Al_2O_3, ZrO_2-CeO_2, and CeO_2 were used for support, it was concluded that alumina outperformed all other catalysts.[21] Schwarz and Pfefferle studied support interactions with Al_2O_3 support and MgO supports, both of which showed combustion below 350 °C, but Al_2O_3 showed greater oxygen mobility across the surface.[23] Cargnello et al. chose and functionalized Al_2O_3 as the support for their CeO_2 coated Pd due to its superior performance, which resulted in exceptional activity below 400 °C.[11] In addition, a collection of other researchers have chosen Al_2O_3 and benefitted from alumina as a quality support.[22,26, 29, 32-37] In their research several different preparation methods were explored. Cargnello reported use of a slurry-type method for preparation

of their reference sample on alumina, as well as calcination temps varying from 500 °C and 850

°C.[11] Miller chose an impregnation method and calcination temps of 500 °C,[21] and Schwarz chose

incipient wetness with a slightly lower calcination temperature of 450 °C.[23] Cargnello also

discussed in their article the commonly observed tendency of PdO decomposing to metallic Pd in

the 650 °C to 800 °C range, mentioning the inferior catalytic performance of metallic Pd to the

PdO phase.[11] In this research project, alumina supported Pd was prepared by methods of slurry,

wet impregnation and incipient wetness. Several different calcination temperatures were also

utilized to aid in selecting the best performing catalysts and for comparison of surface composition.

The second objective of this research was to characterize the prepared catalysts and

determine content of Pd vs. PdO, acknowledging the effects of preparation and catalytic activities

on the surface species. As previously mentioned, Cargnello recognizes PdO as the active Pd

species for methane oxidation.[11] That opinion is shared by others, like Goodman who concludes

that while bimetallic catalysts resist water poisoning, they have substantially lower rates than PdO

phases.[26] It is also the opinion of Stefanov et al. who also concludes PdO to be the active species

in their cobalt bimetallic catalysts.[37] However, there are others who dispute the PdO active phase,

like Bychkov who finds highest catalytic activity over Pd metallic state in methane-rich

conditions,[13] or like Sadokhina who attributes low temperature activity to the evidence of available

metallic Pd sites.[36] In the midst of the Pd vs. PdO active phase dispute are those who hold the

opinion that it is a transition species that displays activity, such as Kinnunen who finds it is the

ratio of Pd to PdO that affects activity with PdOx (x>1) reducing to more catalytic species easier

than stoichiometric PdO.[15] The catalysts in this research were characterized primarily by XPS for

surface composition with supporting characterization including STEM, EDX, and XRD. Surface

composition of the catalysts was compared against their activity and kinetic performance to establish a conclusion regarding the active Pd species.

A kinetics study of the best performing catalyst was the third objective of this research and was necessary in suggesting a catalytic methane oxidation mechanism. Several recent publications also conducted kinetics studies. The particular kinetic studies referenced in this research project are those by Miller et al., Sadokhina et al., and Stefanov et al., who provide adequate details supporting their conclusions.[21, 36-37] All three publications apply an Langmuir-Hinshelwood type model to their kinetic findings and discuss why they chose the models for their research. Miller, who studied support effects on the oxidation of methane arrived at the conclusion that concentration of O_2 is zero-order having no impact on the catalytic rate. Miller also emphasized that kinetics support an inhibitory effect of water, and the importance of both Pd and PdO sites be available for oxidation of methane to occur.[21] Both Sadokhina and Stefanov's work looks at several Langmuir-type surface reactions with respect to methane oxidation.[36-37] Sadokhina corroborates Miller's conclusion that O_2 is zero-order, and adds that CO_2 is also zero-order, but does not offer extensive details on nature of the active Pd surface species.[36] Whereas Stefanov, like Miller points to oxygen mobility across the support, imparting balance to the PdO phase which plays into the kinetics. Stefanov goes on to reject the Eley-Rideal mechanism based on uniform oxygen reaction order and concludes that the oxidation of methane follows a more complex Mars-van-Krevelen model.[37] The kinetics data, in combination with characterization, from this thesis research was compared to both L-H and E-R models to infer the best fit concerning our kinetic findings, and was used to elaborate on the most active Pd surface species.

II.   METHODS

A. Catalyst Preparation

i.   Preparation of 10% Palladium on α-Al$_2$O$_3$ – Varying Calcination Temperatures

Three 10 wt% Pd/Al$_2$O$_3$ catalysts were prepared by the incipient wetness impregnation technique at varying calcination temperatures. A solution was made by dissolving 1.0828 g of palladium (II) nitrate hydrate (Sigma Aldrich, Molar Mass: 230.43 anhydrous basis g/mol) in 3.05 mL of deionized (DI) water. The solution was added to 5.0000 g of aluminum oxide nanopowder, (Sigma Aldrich, Molar Mass: 101.96 g/mol; 13 nm primary particle size; BET surface area, 85-115 m^2/g) by slowly pouring under constant mixing by hand with a small metal spatula. Residual palladium nitrate solution was rinsed out of its beaker using a total of 2.9 mL of D.I. water which was added under mixing to the Pd/α-Al$_2$O$_3$ mixture until the appearance of the mixture resembled small pea-size clumps. An electric kitchen hand mixer attached with only one mixing arm was used to continuously mix the Pd/α-Al$_2$O$_3$ mixture for 10 minutes until the mixture resembled a smooth, sticky paste. The mixture was transferred to a beaker and dried in an air oven overnight at 112-115 °C. The mixture was removed from the oven and placed in a desiccator to cool to room temperature. Sample was weighed on an analytical balance and found to have a mass of 5.2270 g. The dried Pd/α-Al$_2$O$_3$ mixture was divided into 3 even portions. Each portion was crushed and ground with a mortar and pestle and placed in a porcelain crucible. Each mixture was then calcined for 6 hours in a Benchtop Muffle Furnace (Thermolyne make) at corresponding temperatures listed in Table 2.1.

Table 2.1: 10% Pd/α-Al₂O₃ Catalysts – Varying Calcination Temperatures

Catalyst	Calcination Temperature (°C)	Calcination Time	Further Treatment
CSU 1	600	6 hours	none
CSU 1a	750	6 hours	none
CSU 1b	750	6 hours	oxidation
CSU 1c	750	6 hours	reduction
CSU 2	900	6 hours	none
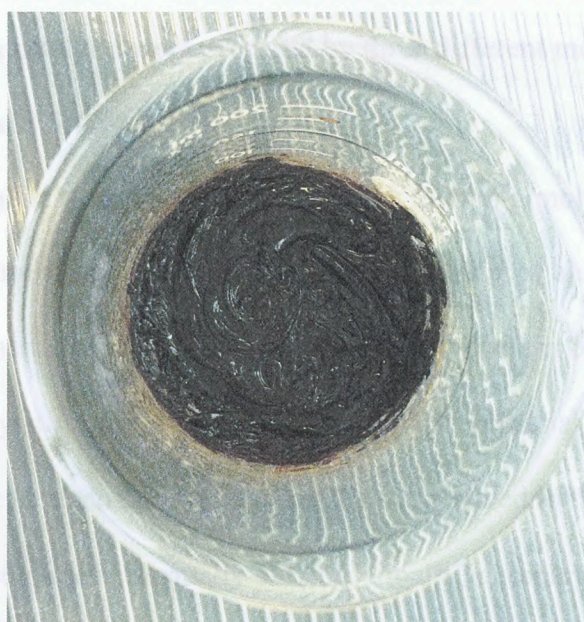
Fig. 2.1: 10% Pd/α-Al₂O₃ Catalyst Before Drying/Calcination

CSU 1b and CSU 1c were obtained through further oxidation and reduction of CSU 1a. For CSU 1b, 0.200g of CSU 1a was placed in the reactor as described in the activity procedure. For CSU 1b, pure oxygen was passed over CSU 1a at 450 °C for 30 minutes, followed by cooling under flow of helium to room temperature. For CSU 1c, pure hydrogen was passed over CSU 1a at 450 °C for 30 minutes, followed by cooling under flow of helium to room temperature. CSU 1b

and CSU 1c were only used for X-ray Photoelectron Spectroscopy (XPS) characterization, while CSU 1, CSU 1a, and CSU 2 were further studied for activity. A sample of CSU 1 was also sent to Georgia Tech for Scanning Transmission Electron Microscopy (STEM) and Energy Dispersive X-ray Spectroscopy (EDS) to determine bulk properties. Activity was performed on CSU 1, CSU 1a, and CSU 2 following the activity procedure described in another section.

ii.   Preparation of 10% Palladium on α-Al$_2$O$_3$ – Varying Methods

Three 10 wt% Pd/α-Al$_2$O$_3$ catalysts were prepared by three different methods: Incipient Wetness, Wet Impregnation, and Slurry.

The incipient wetness catalyst was (Sigma Aldrich, MW: 266.46 g/mol; 40% Pd basis) in 3.0 mL of DI water. The palladium solution was then added to 5.000 g of aluminum oxide (Sigma Aldrich, MW: 101.96 g/mol; nanopowder, 13 nm primary particle size) in 20 μL increments using a micropipette under manually stirring with a small spatula. An additional 1.0 mL DI water was added to the palladium beaker to clean any residual solution and added to the aluminum in 20 μL increments using a micropipette under manually stirring. Finally, another 1.5 mL was added by dropper to achieve the desired dough-like consistency needed for incipient wetness method. The mixture was then mixed with a kitchen hand-mixer for 10 minutes.

The wet impregnation catalyst was prepared by dissolving 0.970 g palladium nitrate dihydrate in 4.0 mL of DI water. To the palladium nitrate solution, 5.000 g of aluminum oxide were added. An additional 2.0 mL of DI water were added to yield the necessary thick mixture needed for the wet impregnation method. The mixture was then stirred with a hand-mixer for 10 minutes.

The slurry method catalyst was prepared by mixing 5.000 g of aluminum oxide in 11.0 mL of DI water to create a slurry. To that mixture a 3.0 mL solution containing 0.970 g of palladium

nitrate dihydrate was added. The resulting mixture was then stirred using a magnetic stirrer for 1.5 hours.

All three solutions were then dried at room temperature; however, the slurry catalyst needed an extra hour of drying in the oven at 105 °C. All three catalysts were then ground with a mortar and pestle and calcined at 500 °C for 6 hours in a Thermolyne Benchtop Muffle Furnace.

Table 2.2: 10% Pd/α-Al$_2$O$_3$ Catalysts – Varying Preparation Methods

Catalyst	Preparation Method	Calcination Temp (°C)	Calcination Time
CSU 5	Incipient Wetness	500	6 hours
CSU 6	Wet Impregnation	500	6 hours
CSU 7	Slurry	500	6 hours
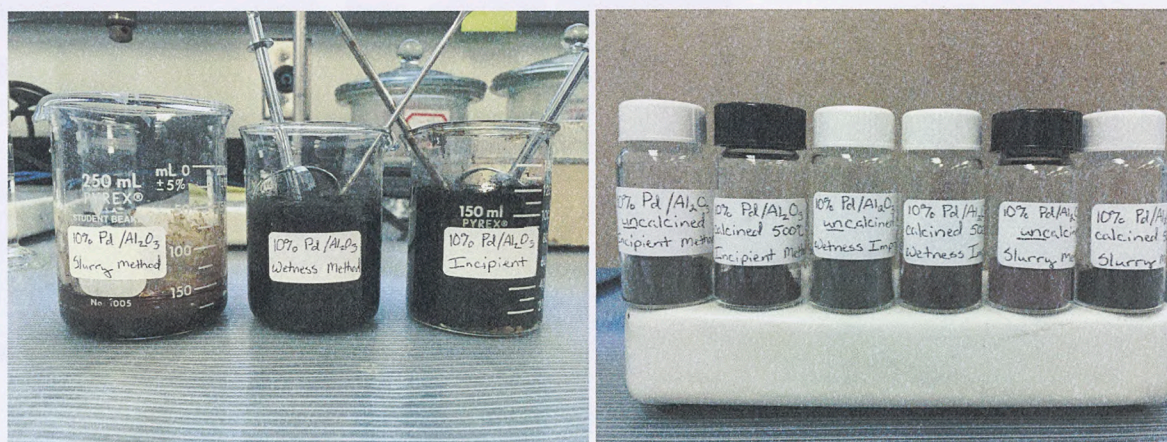
Fig. 2.2: 10% Pd/α-Al$_2$O$_3$ – Varying Preparation Methods

iii.   Preparation of 5% Palladium on γ-Al₂O₃, Vortex Incipient Wetness (Palladium Nitrate Dihydrate Precursor)

A 5 wt% Pd/γ-Al₂O₃ catalyst was made using a palladium nitrate dihydrate precursor. A solution using 2.0 mL of DI water and 0.252 g of palladium nitrate dihydrate was added in 20 µL increments to 1.750 g of gamma phase aluminum oxide nanopowder, (Sigma Aldrich; <50 nm particle size) under vortex mixing set to "3" speed setting for 2 hours. The thick mixture was dried in an oven at 105 °C overnight, crushed with a mortar and pestle, and then calcined at 500 °C for 6 hours in a Thermolyne Benchtop Muffle Furnace. This catalyst was named "CSU 9" and sent to Auburn for XPS characterization.
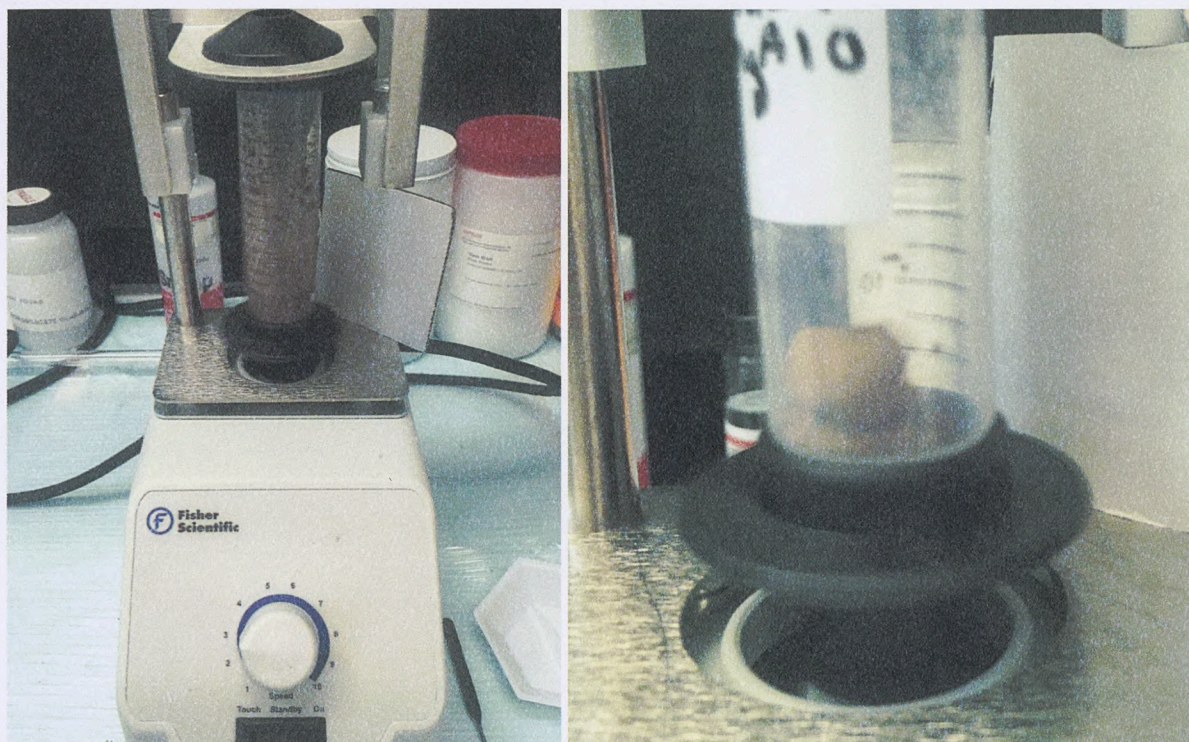
Fig. 2.3: Vortex Incipient Wetness

iv.   **Preparation of 5% Palladium on γ-Al₂O₃, Vortex Incipient Wetness (Palladium**

Nitrate Hydrate Precursor)

A 5 wt% Pd/γ- Al₂O₃ catalyst was made using a hydrate precursor. A solution of 3.0 mL DI

water and 0.328 g of palladium(II) nitrate hydrate, (Sigma Aldrich, MW: 230.43g/mol; anhydrous

basis) was added in 20 μL increments to 1.750 g of gamma phase aluminum oxide nanopowder,

(Sigma Aldrich, <50nm particle size) under vortex mixing set to "3" speed setting for 2 hours. The

resulting "ball" of dough-like mixture was then dried in an oven at 103 °C overnight, crushed with

a mortar and pestle, and then calcined at 500 °C for 6 hours in a Thermolyne Benchtop Muffle

Furnace. This catalyst was then passed through a sieve to achieve particle size of <150 μm, and

named "CSU 10."

Table 2.3: 5 wt% Pd/γ- Al₂O₃

Catalyst	Calcination Temp (°C)	Calcination Time	Variation
CSU 10	500	6 hours	Original
CSU 11	500	6 hours	CSU 10 reacted 80 minutes with 2%CH₄/4%O₂, balance He
CSU 12	500	6 hours	CSU 10 reacted 80 minutes with 2%CH₄/8%O₂, balance He

Fig. 2.4: 5 wt% Pd/γ-Al₂O₃

v.   **Preparation of 20% Palladium on γ- Al₂O₃, Vortex Incipient Wetness (Palladium Nitrate Hydrate Precursor)**

A 20 wt% Pd/γ-Al₂O₃ catalyst was made using a hydrate precursor. A solution of 0.65 mL DI water and 0.432 g of palladium(II) nitrate hydrate, (Sigma Aldrich, MW: 230.43g/mol; anhydrous basis) was added in 20 μL increments to 0.798 g of gamma phase aluminum oxide nanopowder (Sigma Aldrich, <50 nm particle size) under vortex mixing set to "3" speed setting for 2 hours. The resulting "ball" of dough-like mixture was then dried in an oven at 100 °C overnight, crushed with a mortar and pestle, and then calcined at 500 °C for 6 hours in a Thermolyne Benchtop Muffle Furnace. This catalyst was then passed through a sieve to achieve particle size of <150 μm and named "CSU 13."

vi.   Preparation of Standard Grade PdO

Standard grade palladium (II) oxide (Sigma Aldrich) was used for reference. This sample was named "CSU 8."

Table 2.4: Catalyst Inventory: A list of all catalysts with their preparation and characterization methods.

Catalyst	Composition	Prep Method	Precursor	Calcination Temp (°C)	Studies Done
CSU 1	10 wt% Pd/Al$_2$O$_3$	Incipient Wetness	Pd(II) nitrate hydrate	600	XPS, STEM, EDS, Activity
CSU 1a	10 wt% Pd/Al$_2$O$_3$	Incipient Wetness	Pd(II) nitrate hydrate	750	Activity
CSU 1b	10 wt% Pd/Al$_2$O$_3$	Incipient Wetness, Oxidized	Pd(II) nitrate hydrate	750	XPS
CSU 1c	10 wt% Pd/Al$_2$O$_3$	Incipient Wetness, Reduced	Pd(II) nitrate hydrate	750	XPS
CSU 2	10 wt% Pd/Al$_2$O$_3$	Incipient Wetness	Pd(II) nitrate hydrate	900	Activity, XPS
CSU 3	10 wt% Pd/Al$_2$O$_3$	Incipient Wetness, Reacted: 1%CH$_4$/4%O$_2$	Pd(II) nitrate hydrate	600	XPS
CSU 5	10 wt% Pd/Al$_2$O$_3$	Incipient Wetness	Pd(II) nitrate dihydrate	500	Activity, XPS, EDX, SEM
CSU 6	10 wt% Pd/Al$_2$O$_3$	Wetness Impregnation	Pd(II) nitrate dihydrate	500	XPS
CSU 7	10 wt% Pd/Al$_2$O$_3$	Slurry	Pd(II) nitrate dihydrate	500	XPS
CSU 8	Standard PdO	n/a	n/a	n/a	Activity, XPS
CSU 9	5 wt% Pd/γ-Al$_2$O$_3$	Vortex Incipient Wetness	Pd(II) nitrate dihydrate	500	Activity, XPS
CSU 10	5 wt% Pd/γ-Al$_2$O$_3$	Vortex Incipient Wetness	Pd(II) nitrate hydrate	500	Activity, Kinetics, XPS, EDS, SEM, XRD, physisoption, chemisorption, TPR, TPO
CSU 11	5 wt% Pd/γ-Al$_2$O$_3$	Vortex Incipient Wetness, Reacted: 2%CH$_4$/4%O$_2$	Pd(II) nitrate hydrate	500	XPS
CSU 12	5 wt% Pd/γ-Al$_2$O$_3$	Vortex Incipient Wetness, Reacted: 2%CH$_4$/8%O$_2$	Pd(II) nitrate hydrate	500	XPS
CSU 13	20 wt% Pd/γ-Al$_2$O$_3$	Vortex Incipient Wetness	Pd(II) nitrate hydrate	500	Activity, XPS, XRD, EDX, SEM
CSU 14	20 wt% Pd/γ-Al$_2$O$_3$	Vortex Incipient Wetness Reacted: 2%CH$_4$/4%O$_2$	Pd(II) nitrate hydrate	500	XPS
CSU 15	20 wt% Pd/γ-Al$_2$O$_3$	Vortex Incipient Wetness, Helium @ 275°C	Pd(II) nitrate hydrate	500	XPS
CSU 16	Standard PdO	Reacted: 1%CH$_4$/4%O$_2$	n/a	500	XPS

B. Activity and Kinetics Study

i. Catalytic Activity Procedure

The catalytic activity was monitored by passing a reaction gas mixture over a stationary catalyst bed, packed in a quartz tubular reactor between layers of glass wool. A picture of the catalyst bed is pictured in Figure 2.5.
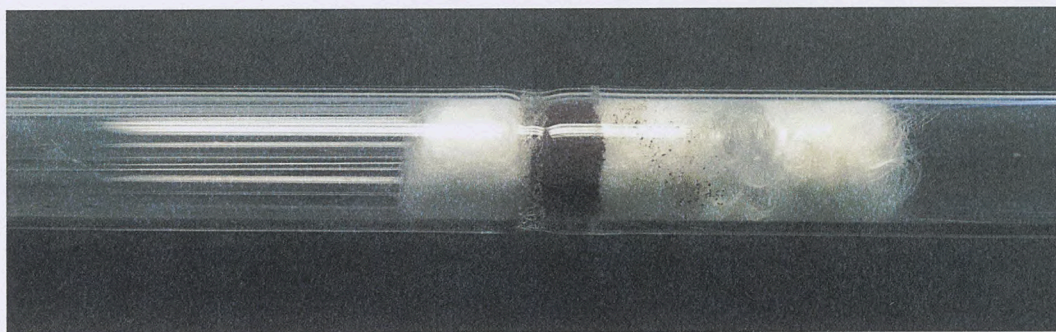
Fig. 2.5: Catalyst Bed in Reactor

The reactor was first packed with a layer of silanized glass wool (Supelco), followed by 0.200 g of catalyst, followed by another layer of glass wool, followed by a layer of 20-30 borosilicate 3 mm glass beads (Sigma-Aldrich), followed by a final layer of glass wool to hold the bed stationary while allowing uninhibited gas flow. A gas mixture was passed through 1/8" diameter copper tubing, feeding into a Mass Flow Controller (Aalborg, GFC17) at a flow rate of 1.0 L/min. The gas mixture then travelled through a coil of more copper tubing to ensure proper mixing of the gas before entering the reactor which was placed in a temperature-controlled horizontal tube furnace. The gas mixture passed over the catalyst bed and the effluent gas exited the reactor through a plastic tubing fitted with glass T-junction and a rubber septum. A syringe was inserted through the septum to draw out samples of the effluent gas mixture. The temperature of the reactor was

monitored using an Omega thermocouple thermometer sheathed in a glass tube inserted into the entrance of the reactor, the tip situated directly at the catalyst bed. A picture of the reactor assembly is shown in Figure 2.6.
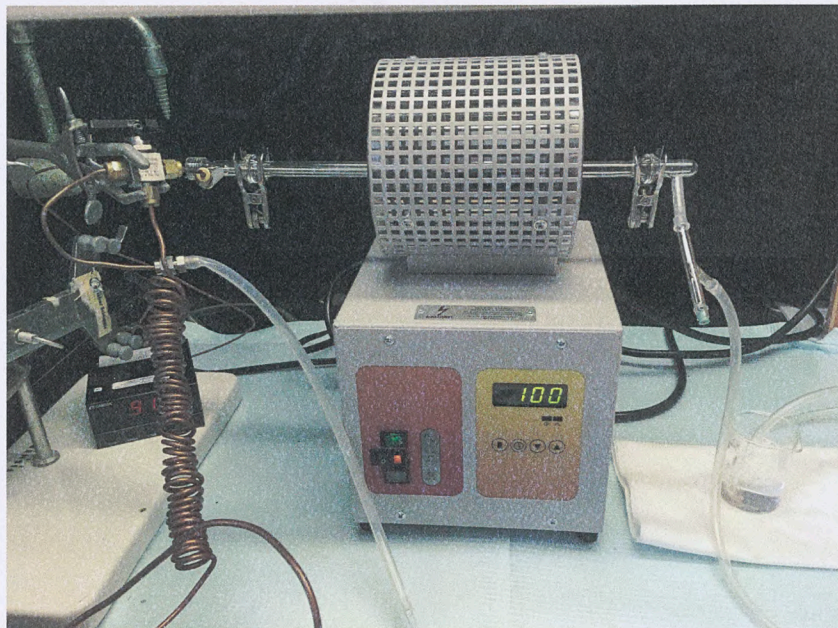
Fig. 2.6: Reactor Assembly
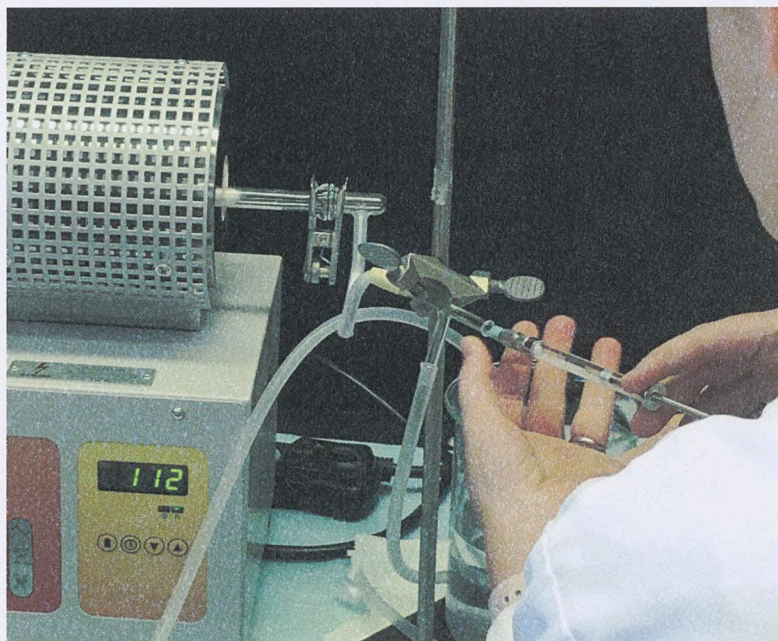
Fig. 2.7: Drawing a Sample

The sampled effluent gas was injected into a gas chromatograph (Buck Scientific Model 310) fitted with a 6 ft. shincarbon packed column and a Thermal Conductivity Detector (TCD). The GC data was analyzed using PeakSimple software under the following temperature parameters: hold initial temperature for 5 minutes at 40 °C, then ramp at 20°C/min, until maximum temperature of 180 °C is reached, hold for 3 minutes, and then cool down to 40°C. The full cycle of one GC analysis takes 15 minutes to complete. A sample chromatogram produced by "PeakSimple" software is shown in Figure 2.8.
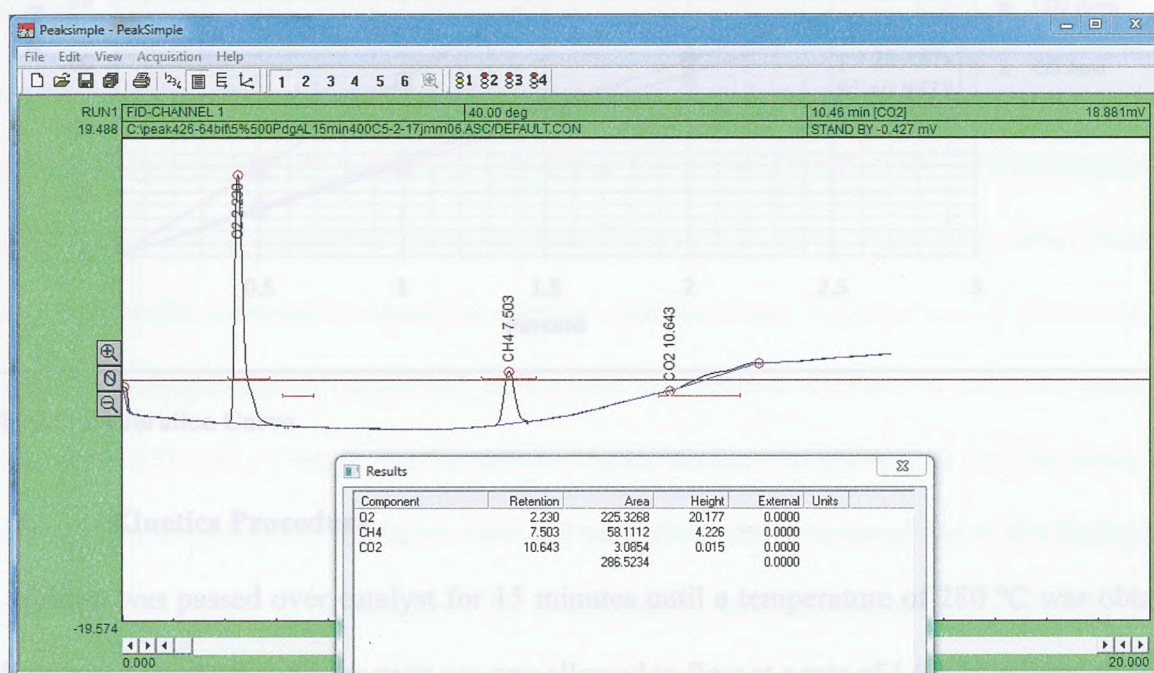
Fig. 2.8: PeakSimple Chromatogram

The retention time of the peaks indicates the identity of the compound, as each species has a varying affinity for the column and therefore travels its length at a different velocity, while the area of the peak is directly related to the concentration of the gas mixture. Prior to catalytic studies, a calibration curve was constructed by injecting varying volumes of a standard gas mixture of

1% CO/1% CH₄/1% CO₂ to provide a correlation between area and effluent gas concentrations. The calibration curve is given in Figure 2.9.

Calibration of Standard Gas Mixture

$y = 55.047x$
$R^2 = 0.9986$

$y = 30.518x$
$R^2 = 0.9979$

♦ CH4 Area

■ CO2 Area

▲ CO Area

$y = 28.487x$
$R^2 = 0.9979$

Peak Area (y-axis)

Percent (x-axis)
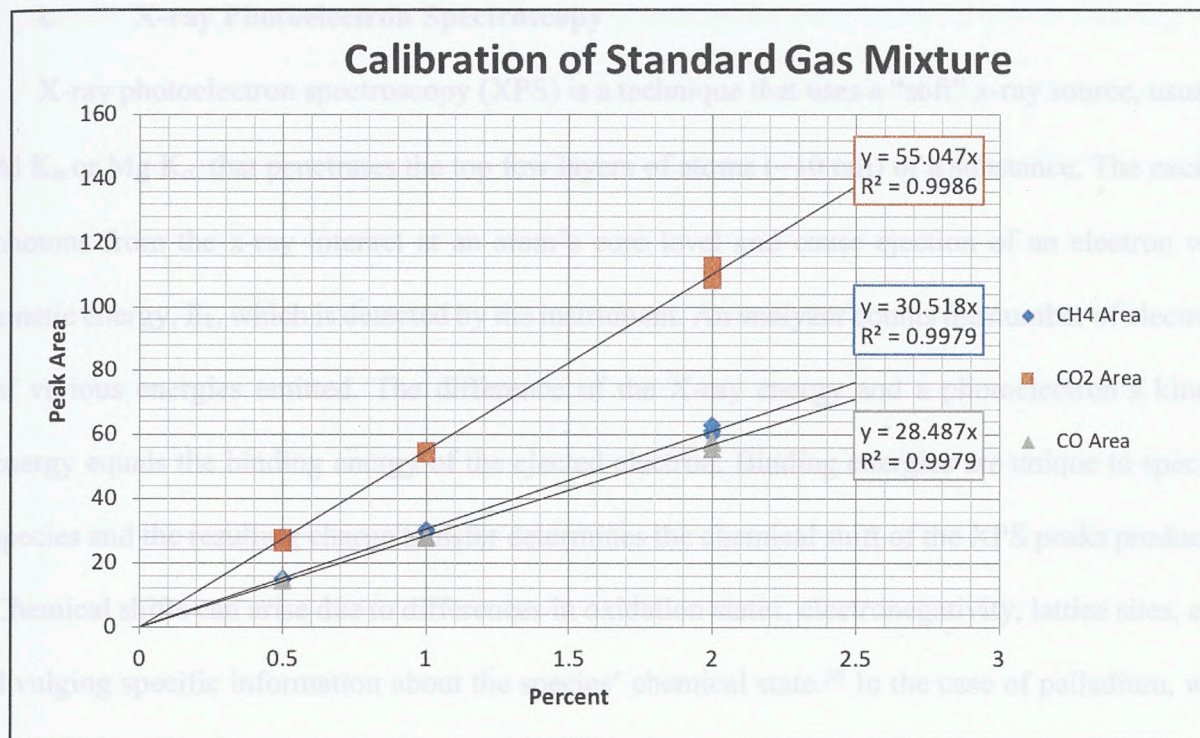
Fig. 2.9: Calibration Curve

ii.   Kinetics Procedure

Helium was passed over catalyst for 15 minutes until a temperature of 280 °C was obtained. Helium was turned off and a reaction gas was allowed to flow at a rate of 1.0 L/min through reactor assembly and over the catalyst. Samples of 0.5 mL product mixture were drawn out from the end of the reactor using a SGE Push-pull with Luer Lock 1mL syringe at 5, 20, 35, 50, 65 and 80 minutes of reaction time. A fixed volume of the gas mixture collected in the syringe was injected into the GC for analysis.

C. Characterization Techniques

i.   X-ray Photoelectron Spectroscopy

X-ray photoelectron spectroscopy (XPS) is a technique that uses a "soft" x-ray source, usually Al K_α or Mg K_α, that penetrates the top few layers of atoms (~10 nm) of a substance. The excited photons from the x-ray interact at an atom's core level and cause ejection of an electron with kinetic energy, E_k, which is detected by the instrument. An analyzer counts the number of electrons of various energies emitted. The difference of the X-ray energy and a photoelectron's kinetic energy equals the binding energy of the ejected electron. Binding energies are unique to specific species and the resulting charge transfer determines the chemical shift of the XPS peaks produced. Chemical shifts can arise due to differences in oxidation states, electronegativity, lattice sites, etc., divulging specific information about the species' chemical state.[38] In the case of palladium, with an electron configuration of $[Kr]5s^24d^8$, XPS x-rays will interact with the 3d electrons resulting in a peak in the 335-340 eV range. Further deconvolution dissects the Pd3d peak into the minor shifts that occur due to changes in oxidation state and can infer percent composition of the particular Pd species that are present in the sample. XPS is intended to analyze surface composition to a depth of ~10 nm (100 Å), however profiling can be achieved at depths of 100-200 nm (1000-2000 Å) through a process referred to as "sputtering," in which a beam of Ar^+ ions is used to drill further into the sample and analyze slightly further below the surface.

XPS is of particular use in the determination of metal oxides, which can occur either precisely stoichiometric (e.g. PdO), or can show stoichiometric variability over a range of compositions (e.g. PdO_x). Transition elements with their variable oxidation states frequently show in their oxides and sulphides this non-stoichiometric behavior.[38] In XPS terms, these non-stoichiometric oxides are

sometimes referred to as "native oxides" (e.g. Pd Native or PdNtv). Characterization by XPS for

catalysts in this study was performed at Auburn University's Center for Advanced Vehicle and

Extreme Environment Electronics (Cave[3]). The procedure for analysis by XPS is as follows:

Photoemission measurements were performed in a load-locked Kratos XSAM 800

surface analysis system equipped with a hemispherical energy analyzer. The base

pressure of this ion- and turbo-pumped system was 8×10^{-9} torr as read on a nude

ion gauge. The XPS analyzer was a 127 mm radius double-focusing concentric

hemispherical energy analyzer (CHA) equipped with an aberration compensated

input lens (ACIL). XPS spectra were recorded in the fixed analyzer transmission

(FAT) mode with a pass energy of 80 eV, appropriate for acquisition of medium

resolution, high signal-to-noise spectra. The magnification of the analyzer in the

FAT mode was selected to collect electrons from the smallest allowable ($5 \ mm^2$)

area on the specimen. The resolution of the instrument at the operating parameters

was measured from FWHM of the $Ag3d_{5/2}$ peak to be 1.0 eV. The XPS energy scale

was calibrated by setting the $Ag3d_{5/2}$ line on clean silver to exactly 368.3 eV

referenced to the Fermi level. Due to specimen charging during X-ray irradiation,

the energy axis of each XPS spectra has been shifted to make the C1s binding

energy line equal to 285.0 eV, which is a standard hydrocarbon energy (C-H and

C-C bonds) used to reference charge affected materials. The potential measured

on a typical sample was 0.5 V. The photoelectrons were excited by a water-cooled,

conventional (i.e., non-monochromatic) dual anode X-ray gun equipped with an Al

window. The angle of the incidence of the x-ray beam with the specimen normal

was 51.5^o. MgK_α (1253.6 eV) radiation was used exclusively. In cases when the

peaks were low in amplitude, the Savitsky-Golay smoothing routine was used in order to help determine the peak binding energies. The XPS surface composition was calculated based on the Scofield cross-sectional values accounting for the instrumental transmission function in the FAT mode of operation. The specimen was pressed into double-sided carbon tape to a thickness which insured that the emitted photoelectrons would originate only from the specimen.[39]

ii.   X-ray Diffraction

X-ray diffraction is a useful method for identifying the crystalline phases of a catalyst. The sample is hit with x-rays over a range of angles. The resulting elastic scattering of the x-ray photons is directly related to the spacing in the crystal lattice. It uses Bragg's Law: $n\lambda = 2dsin\theta$, where n=1, 2,..., d is the spacing between atomic planes in the crystalline phase and θ is the diffraction angle. Intensities of the diffracted x-rays are plotted as a function of the diffraction angle (2θ).[14] Well-defined diffraction peaks are associated with high-quality crystalline structure while diffuse diffraction peaks are associated with more amorphous structures. Because each substance has its own unique set of d-spacings, the diffraction peaks can be used to identify the compound and the phase that is present in the bulk of the sample. The 2θ values can be matched up against the International Center for Diffraction Data (ICDD) database for identification.[14] The diffraction peaks of interest for this research are those for metallic Pd, PdO and Al_2O_3. The ICDD shows matches for unsupported pure PdO having a strongest line at a 2θ of 33.837°. This data is corroborated by other researchers conducting XRD on supported PdO catalysts.[27, 40-42] The strongest peak for metallic Pd is expected to occur at a 2θ of about 40° and that of Al_2O_3 at a 2θ of about 46° and 67°.[21, 41-42]
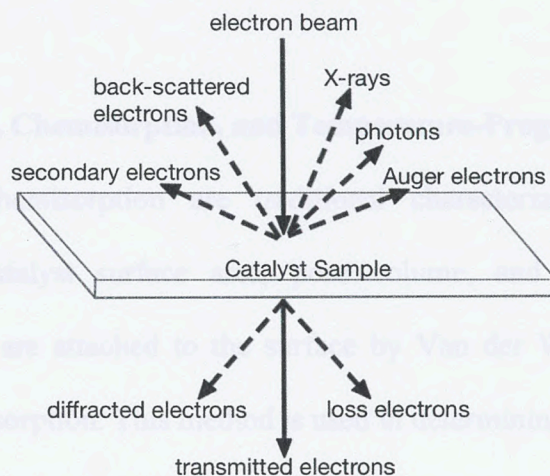
XRD on CSU 13 and 14 was conducted in the Materials Science and Engineering Department of Auburn University. The instrument used was a Bruker D8 Discover diffractometer fitted with a 1D detector using a Cu radiation source at 40 kV and 40 mA. Catalyst samples of approximately 0.1g were prepared on a glass plate using another glass plate to press flat. The samples were then irradiated at a 2θ range from 5-90° at a speed of 8°/min.

X-ray analysis of CSU 10, standard PdO and standard γ-Al_2O_3 was done in the Department of Geosciences at Auburn University on a Bruker AXS D2 Phaser using a Cu radiation source at 30kV and 10mA. Samples were irradiated at a 2θ range from 15-90° at a speed of 2.4°/min. Samples were either applied to a zero-plate or to double-sided tape to ensure even application to the XRD slide.

iii. Scanning Electron Microscopy, Scanning Transmission Electron Microscopy, and Energy Dispersive X-Ray Spectroscopy

Two types of electron microscopy were used in this research. The first of these is Scanning Transmission Electron Microscopy (STEM). Transmission electron microscopy in principal works very similar to optical microscopy. However, instead of optical lenses, TEM uses electromagnetic ones. When an electron beam is directed at a thin preparation of the catalyst sample the resulting transmitted electrons are magnified by the electromagnetic lenses. Contrasts in the image are a result of different scattering processes that arise due to varying interactions with different atoms in the sample. Figure 2.10 illustrates the different types of scattering that can result when an electron beam hits a sample. Typically, the thicker electron density of the catalytic metal will appear darker than its support, providing a good visual image of the metal dispersion.[14] Scanning electron transmission microscopy (STEM) works very similar to TEM, however STEM primarily uses the transmitted electrons to form the image. In STEM a small electron probe of focused

electrons scans across the sample. As the detector receives a signal, an image is formed based off that signal as a function of the probe's position. Using a bright-field detector, the transmitted electrons can be collected on an axis.[43] STEM studies along with EDS on CSU 1 were conducted at Georgia Institute of Technology.

electron beam

back-scattered electrons

X-rays

photons

secondary electrons

Auger electrons

Catalyst Sample

diffracted electrons

loss electrons

transmitted electrons

Fig. 2.10: Types of Scattering

The second type of microscopy is Scanning Electron Microscopy (SEM). In this characterization technique, a high-energy electron beam is scanned across the surface of the catalyst sample, producing low energy secondary electrons. Some of the electrons from the beam will strike atomic nuclei and bounce back which is known as "back-scattering". Back scattered electrons divulge information regarding surface topography and atomic number. Because secondary electrons originate from the surface and back-scattered electrons come from the bulk, the resulting SEM image is 3-dimensional.[14] SEM and EDS for CSU 5, 10 and 13 were conducted at Auburn University.

Electron Dispersive Spectroscopy (EDS) is obtained in correlation with SEM and/or TEM since it is a detector commonly fixed to both. When the electron beam hits the sample, atoms

whose inner-shell electrons have been promoted to a higher energy state release energy as their electrons drop back down to inner shell vacancies. This relaxation process can produce either low-energy Auger electrons or X-rays. Because atomic energy levels are well-defined, the energy and associated wavelengths identify the atomic species that emitted it. This provides an adequate representation of the bulk composition of the catalyst sample.[43]

iv. Physisorption, Chemisorption, and Temperature-Programmed Techniques

Physisorption and chemisorption are traditional characterization methods that yield information regarding catalyst surface area, pore volume, and pore size distribution. In physisorption, molecules are attached to the surface by Van der Waals interactions with low corresponding heats of adsorption. This method is used in determining total surface area and pore volume. Chemisorption, however, involves breaking and creation of adsorption bonds with heats of adsorption, higher than those of physisorption. Chemisorption is used for measuring the crystallite size (particle size), active surface area and metal surface area.[14]

Temperature-programmed techniques measure the reactivity of a solid as a function of temperature under controlled conditions. The temperature at which species reacts on the surface reflects the bond strength of the species. The techniques used in this research are Temperature Programmed Reduction (TPR) and Temperature Programmed Oxidation (TPO). TPO and TPR give a good reflection of what the catalyst undergoes during calcination. In both techniques, a mixed gas of 10% oxygen in helium/argon or a 10% hydrogen gas in helium/argon is passed over the catalyst and the temperature is ramped up. The amount of hydrogen or oxygen adsorbed at different temperatures are determined by a thermal conductivity detector. Physisorption (by BET

method), chemisorption, TPO and TPR for this research were performed at Georgia Institute of Technology and the procedures were as follows:

Chemisorption experiments including temperature programmed reduction (TPR) and pulse CO chemisorption were conducted in Micromeritics AutoChem II 2920. For each TPR experiment, approximately 30 mg of sample was placed on top of a small bed of quartz wool in a quartz U-tube. In regard to the TPR experiment, the material was pretreated in 30 mL/min of He (Airgas, UHP) at 110°C for 1 hours to remove preadsorbed species. The sample was then cooled to 30°C and 20 mL/min of 10% H₂ balance Ar was flown over the sample. The furnace was heated to 500 °C at 5 °C/min while under the flow of 10% H₂/Ar. The outlet gas passed through a liquid acetone/nitrogen trap, and then passed through a Thermal Conductivity Detector (TCD).

For each TPO experiment, approximately 30 mg of sample was placed on top of a small bed of quartz wool in a quartz U-tube. In regard to the TPO experiment, the material was pretreated in 30 mL/min of He (Airgas, UHP) at 110°C for 1 hours to remove pre-adsorbed species. The sample was then cooled to 30°C and 20 mL/min of 10% O₂ balance He was flown over the sample. The furnace was heated to 500°C at 5°C/min while under the flow of 10% O₂/He. The outlet gas passed through a Thermal Conductivity Detector (TCD).

CO with Reduction:

Approximately 30 mg catalyst sample was placed in the quartz tube held in place by quartz wool. The material was pretreated in 30 mL/min of He (Airgas, UHP) at 110°C for 1 hour to remove pre-adsorbed species. During the reduction step (see TPR for gas flow rates) the sample was heated to 450°C at 5°C/min and held for 30 min. The sample was then cooled to 400°C where He began to flow for 30 min to remove all adsorbed species. Afterwards the sample was cooled down to 30°C to begin pulse CO testing. Doses of 10% CO/He (Airgas) were passed over the sample and analyzed in the TCD. Once saturation was reached, He was flowed over the sample for 30 min to remove physisorbed species (50 mL/min). Finally, a second round of pulses was conducted to verify if there were any physisorbed species adsorbed, which was taken into consideration when calculating the active metallic surface area.

CO without Reduction:

Approximately 30 mg catalyst sample was placed in the quartz tube held in place by quartz wool. the material was pretreated in 30 mL/min of He (Airgas, UHP) at 110°C for 1 hours to remove pre-adsorbed species. Afterwards the sample was cooled down to 30°C to begin pulse CO testing. Doses of 10% CO/He (Airgas) were passed over the sample and analyzed in the TCD. Once saturation was reached, He was flowed over the sample for 30 min to remove physisorbed species (50 mL/min).

Finally, a second round of pulses was conducted to verify if there were any physisorbed species adsorbed, which was taken into consideration when calculating the active metallic surface area. "[44]

III.   RESULTS AND DISCUSSION

A. Results

i.   STEM and SEM

CSU 1 was sent to Georgia Institute of Technology for STEM. This catalyst was prepared by incipient wetness method with a calculated 10% (w/w) of $Pd/\alpha-Al_2O_3$. Figure 3.1 shows a magnified STEM image of the catalyst. The bright areas in the produced image correspond to Pd while the dull gray areas correspond to the support, Al_2O_3. This image confirms that initial preparation method was depositing nanoparticles on the alumina surface.
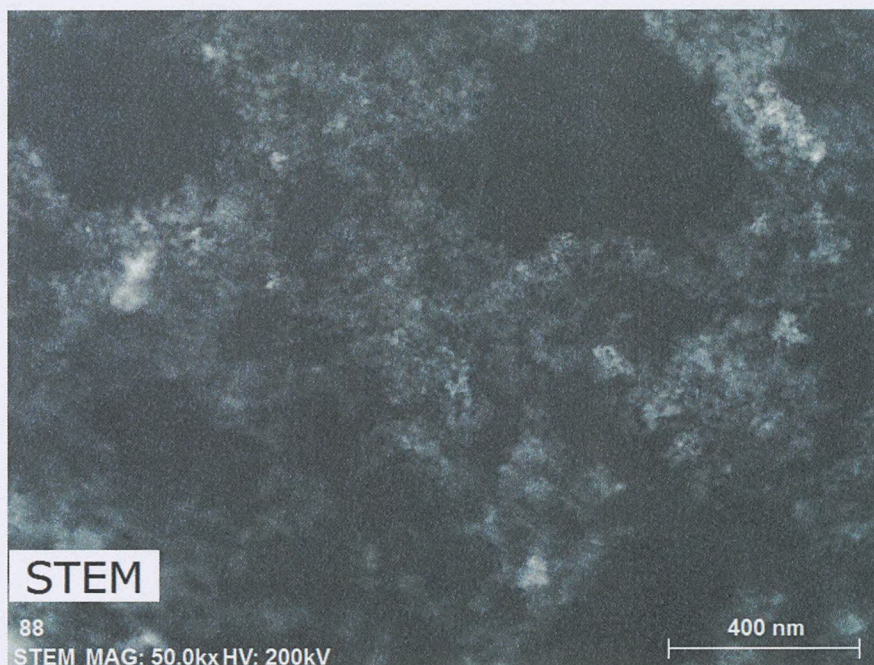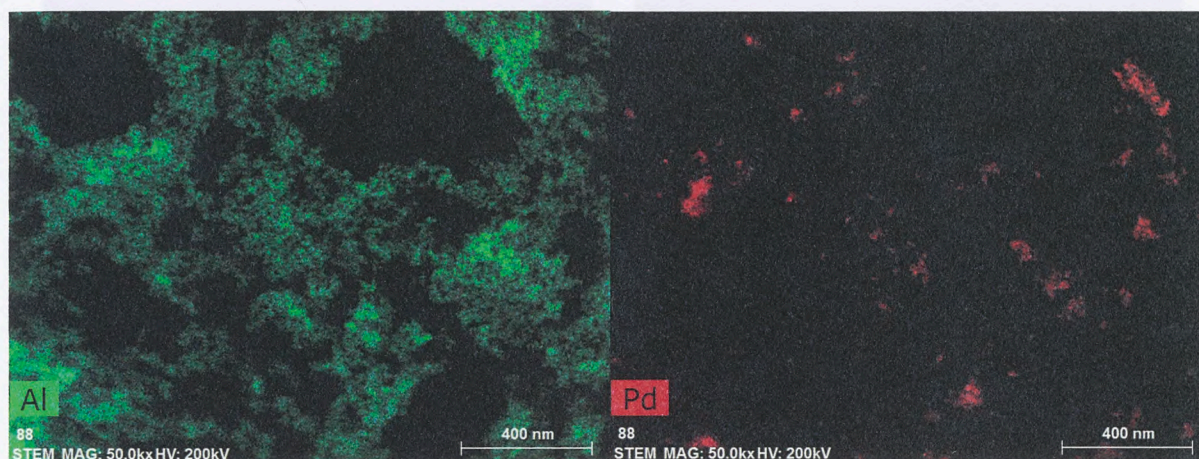

**Fig. 3.1: STEM of 10% $Pd/\alpha-Al_2O_3$**

The contrast images in Figure 3.2 give better clarity on the dispersion of the Pd nanoparticles. In these images, green areas represent the alumina support and the red areas reveal the position and sizes of the Pd nanoparticles. Size of the particles in this first prepared catalyst shows significant variation, with some particles being smaller, but also some Pd showed agglomeration into

unfavorable large particles. Large particles are problematic in that available Pd surface area is decreased along with Pd-support interactions. This variation in particle size provided some of the reason behind seeking to improve the preparation method, on the suspicion that the catalyst was not being stirred thoroughly enough nor for a long enough period of time to ensure optimal dispersion. XPS results on this catalyst would provide further evidence of poor dispersion.

Fig. 3.2: Contrast STEM of 10% Pd/α-Al₂O₃

In Fig 3.3, a specific Pd particle was isolated and the edge of the particle was further magnified through high-angle annular dark field (HAADF) STEM. In the highest resolution, the bright dots reveal the crystal lattice structure of the Pd atoms. However, moving towards the edge of the particle, the uniform structure disappears into an amorphous region, which could possibly represent surface oxides.
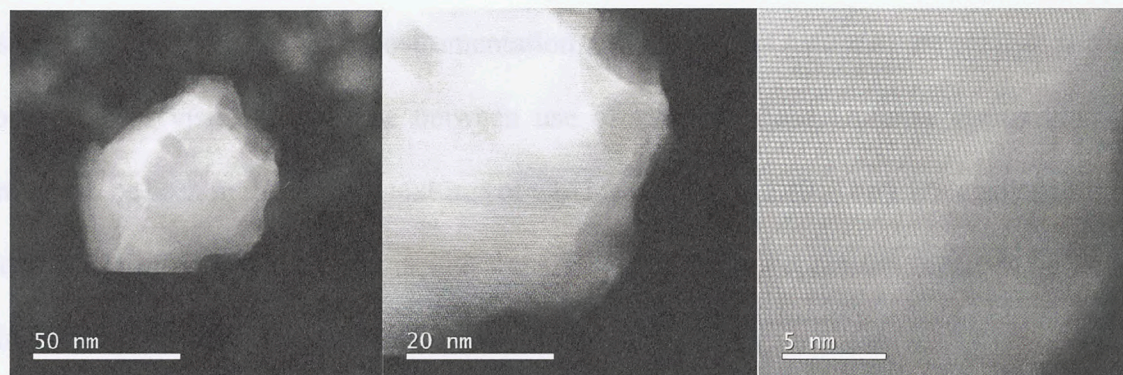
Fig. 3.3: HAADF STEM Images of Pd Particle

Further evidence of crystal lattice can be seen in Figure 3.4, which shows a side-by-side comparison of HAADF and Bright-field STEM. Subtle parallel hashed lines in both images show areas with crystalline order, which mostly correspond to the bright spots, or the Pd particles. Some order can be seen in the alumina support as well.
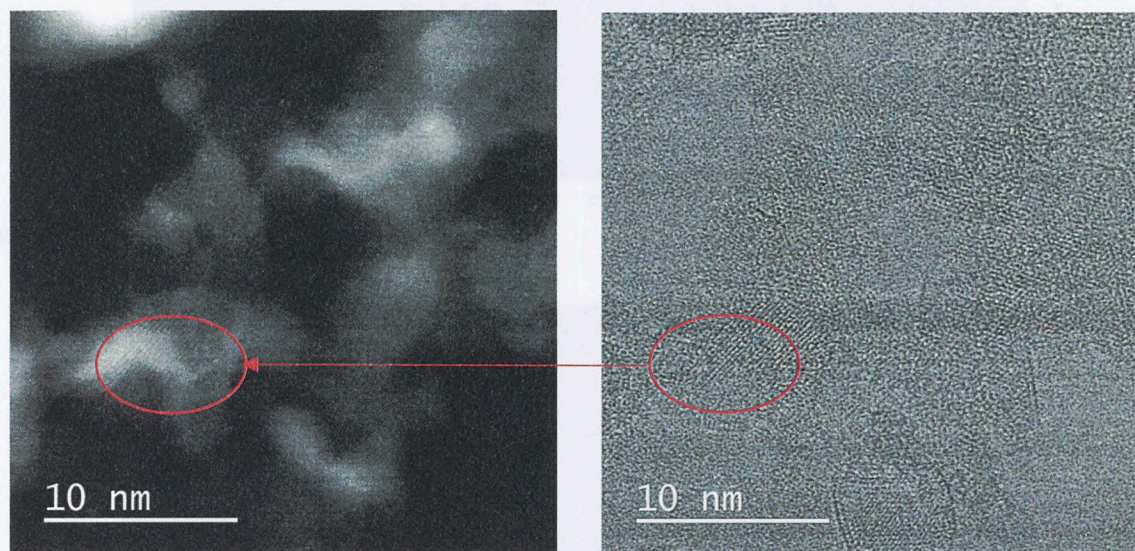

Fig. 3.4: HAADF and Bright-field STEM Images of Pd Particles. HAADF (right) and Brightfield (left)

CSU 5 and 10 were sent to Auburn for SEM and EDS. The CSU 5 catalyst shown in Figure 3.5 was prepared on alpha-aluminum oxide by incipient wetness at a calculated weight percent of 10% Pd/Al_2O_3. The CSU 10 catalyst shown in Figure 3.6 was prepared on γ-alumina by incipient wetness vortex method at a calculated weight percent of 5% Pd/γ-Al_2O_3. The SEM image of CSU 10 is slightly distorted due to the instrumentation, but the porous nature of the catalyst surface can be observed. A visible difference between use of gamma phase alumina versus alpha phase alumina can be seen in the surface textures of CSU 5 versus CSU 10. The EDS analysis from these same samples provides more insight into the efficacy of their preparation methods by looking at the bulk composition of the catalysts.
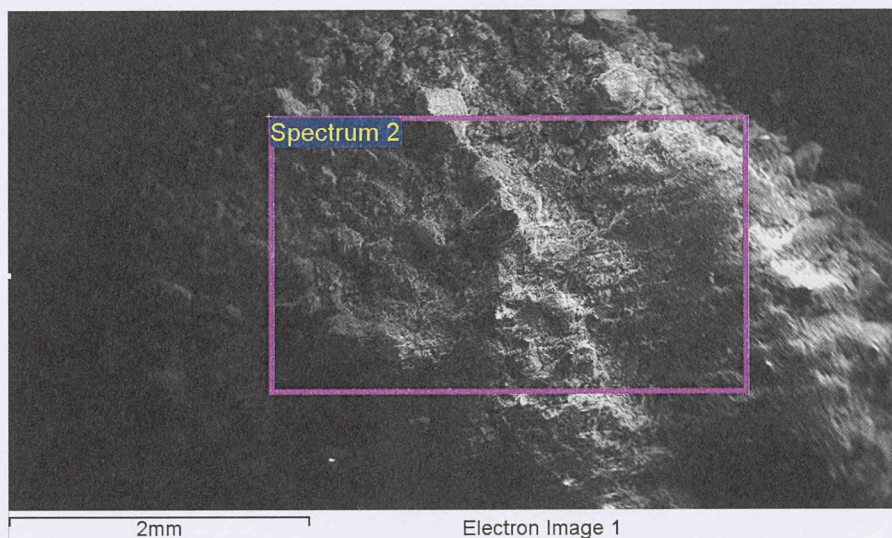
Fig. 3.5: SEM image of 10% Pd/α-Al₂O₃

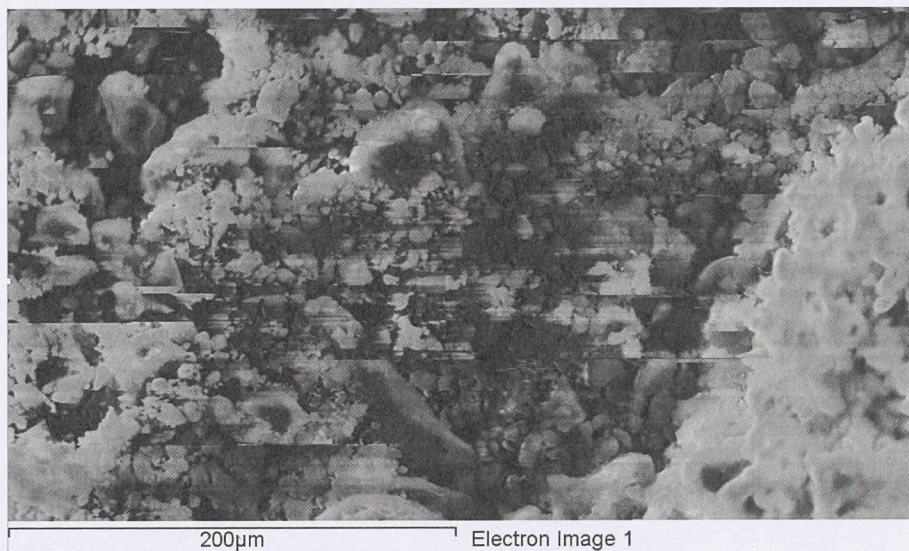Fig. 3.6: SEM image of 5% Pd/γ-Al₂O₃

ii.   EDS

EDS tests were run on three different areas of CSU 5 (10% Pd/α-Al$_2$O$_3$) to determine bulk composition of the catalyst. The EDS corresponding to the area in Fig. 3.5 is demonstrated in Figure 3.7. The composition average of the 3 areas found an atomic percent of 1.26% which corresponds to a weight percent of 6.41%. Because this catalyst was prepared as 10 wt% Pd, the EDS results raised concern as to the efficacy of the preparation method since a significant amount

of Pd was missing in the final catalyst, resulting in an error of 36%. One suspected cause for loss was that the hand-mixer used in preparation was not able to reach crevices in the mixture beaker, causing some palladium to adhere to the beaker and not transfer to the crucible for calcination into the final product. Some Pd could have also been lost by adhering to the mixing arm itself. Another suspected loss of Pd was the use of a dropper to incorporate the aqueous Pd precursor into the support. A dropper delivered approximately 50 μL per drop and at inconsistent intervals which could have increased the amount of Pd adhering to the side of the beaker and on the mixing arm rather than incorporating into the support.
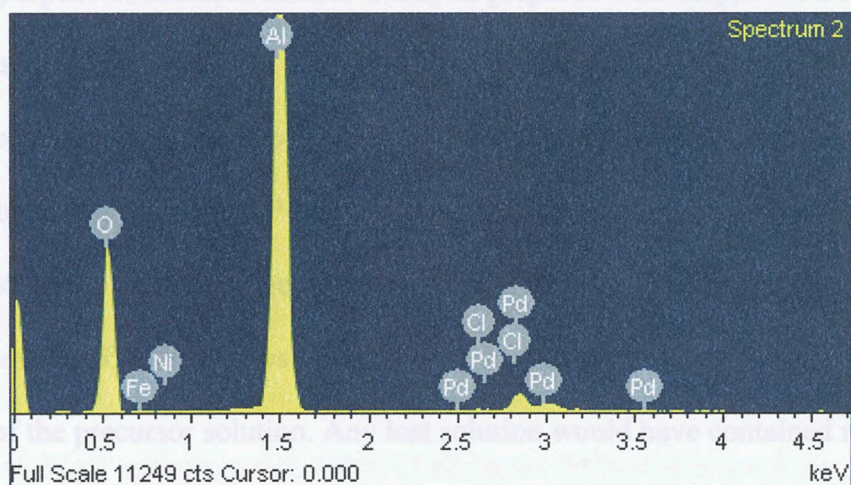

Fig. 3.7: EDS of CSU 5. Prepared as 10 wt% Pd, but analyzed as only 6.41 wt% Pd.

EDS on CSU 10 is shown in Figure 3.8. This catalyst was prepared as 5 wt% Pd/γ-Al$_2$O$_3$ using an improved incipient wetness method using a vortex mixer over a duration of 2 hours and incorporating the precursor using a micropipette to deliver 20 μL per drop. An average of 2 scanned areas resulted in a 0.93 atomic percent, which corresponded to a 4.3 wt% Pd. This analysis resulted in a weight percent much closer to the targeted weight percent, with a 14% error compared to the previous method with a 36% error. This improvement was attributed to the changes made to the preparation procedure.
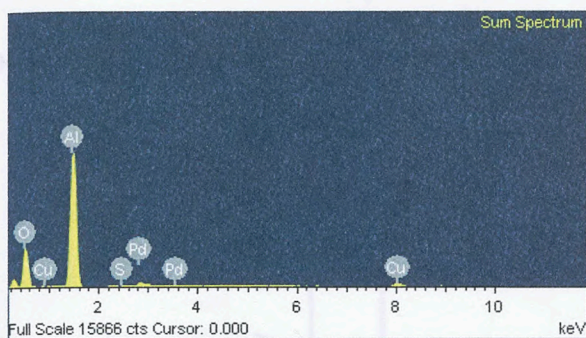
Fig. 3.8: EDS of CSU 10. Prepared as 5 wt% Pd/γ-
Al$_2$O$_3$ and analyzed as 4.3 wt%
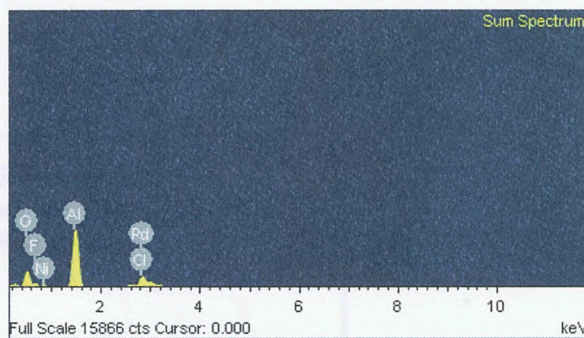
Fig. 3.9: EDS of CSU 13. Prepared as 20 wt% Pd/γ-
Al$_2$O$_3$ and analyzed as 14.74 wt%

EDS on CSU 13 is shown in Figure 3.9. This catalyst was prepared as 20 wt% Pd/γ-Al$_2$O$_3$

mostly for the purpose of characterization. Catalysts prepared with very low Pd loadings result in

increased "noise" in spectroscopic analysis, so a higher Pd loading was prepared to better

determine percentages of surface compounds which could then be inferred on the lower Pd

loadings. The bulk composition of Pd in this catalyst was found to be 2.95 at% and 14.74 wt%,

which was a 26% error from the targeted preparation of 20% Pd. This catalyst was prepared in the

same method as the 5% Pd catalyst, so the loss of Pd this time was attributed to the high

concentration of the precursor solution. Any lost solution would have contained more Pd than the

solution prepared for the 5% Pd catalyst.

iii.   XPS

All XPS studies were conducted at the NSF Center for Advanced Vehicle and Extreme

Environment Electronics (CAVE[3]) at Auburn University. A specimen containing Pd would

produce a peak at a binding energy (BE) of 335-340eV as shown in the XPS of CSU 13 in Figure

3.10.[38] The concentration of the surface species would result in greater intensity, thus catalysts

with much lower Pd loadings would result in lower resolution peaks than the one observed in Fig.

3.10. Once identified, the Pd peak could then be further deconvoluted to distinguish the types and

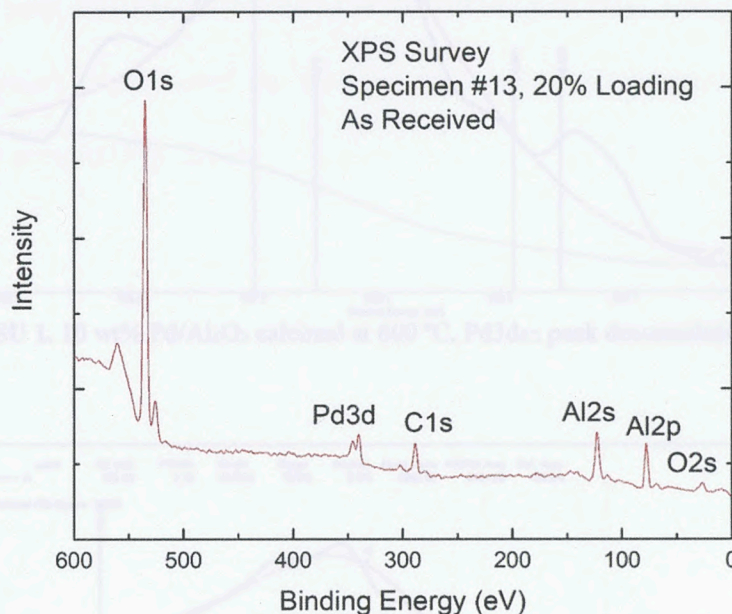percent of Pd phases present on the surface.

Fig. 3.10: XPS of CSU 13

XPS on CSU 1 found the total surface Pd to be 2.19 wt%. The deconvoluted Pd3d$_{5/2}$ peak

for CSU 1, prepared as 10 wt% Pd/α-Al$_2$O$_3$, is shown in Figure 3.11. The entire peak is centered

over a BE of 336.77eV indicating that 100% of Pd on the surface is in the form of stoichiometric

PdO. This is the amount present in the upper 10 nm of the catalyst. Upon sputtering with Ar$^+$ to a

depth of 1000Å (100 nm), the peak shifts to concentrate over a BE of 336.0eV indicating a shift to

100% "Pd native oxide" (PdNtv) and/or elemental Pd as shown in Figure 3.12. Further sputtering

to a depth of 2000Å (200 nm), maintains a composition of PdNtv and/or elemental Pd (Figure
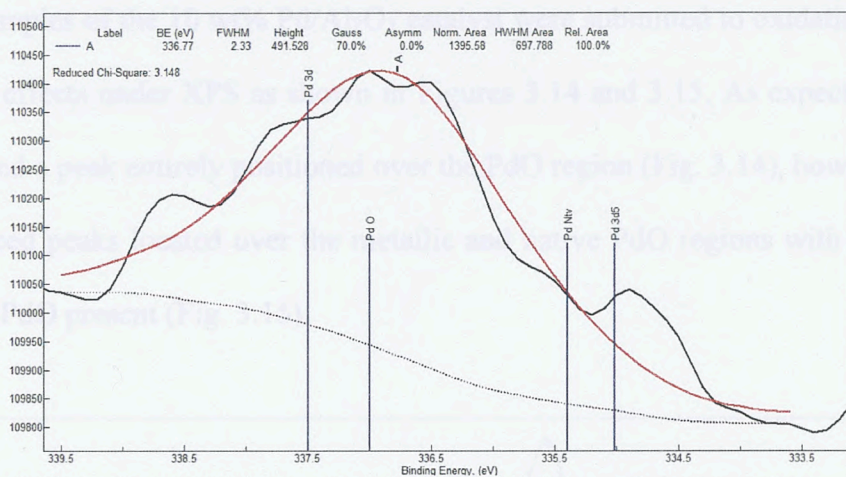
3.13).

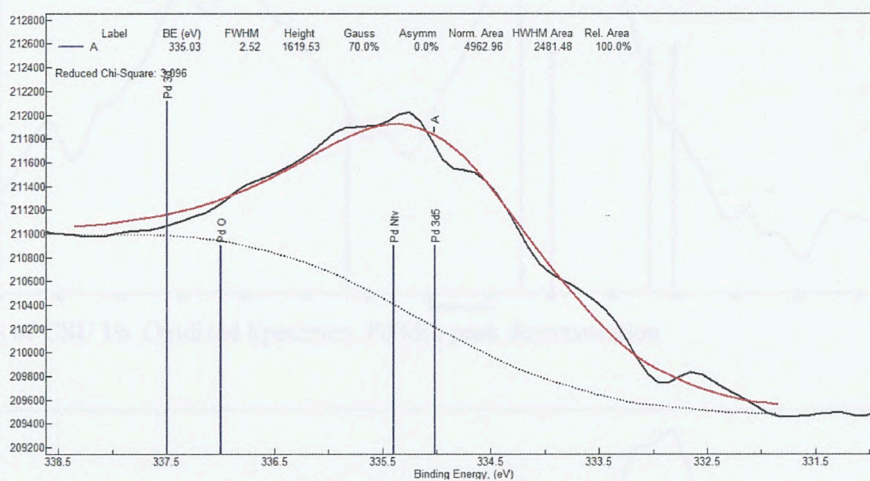**Fig. 3.11: XPS of CSU 1.** 10 wt% Pd/Al$_2$O$_3$ calcined at 600 °C. Pd3d$_{5/2}$ peak deconvolution

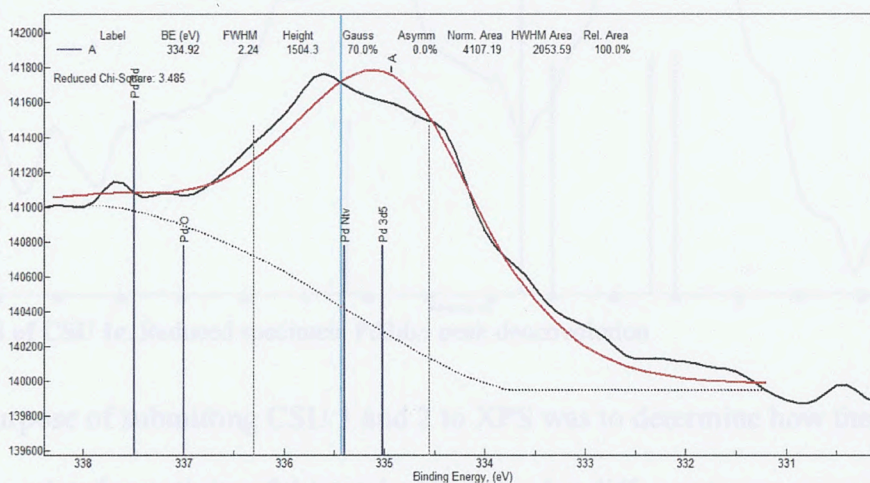**Fig. 3.12: XPS of CSU 1 - Sputtered 1000Å.** Pd3d$_{5/2}$ peak deconvolution

Fig. 3.13: XPS of CSU 1. Sputtered 2000Å. Pd3d$_{5/2}$ peak deconvolution

Two samples of the 10 wt% Pd/Al$_2$O$_3$ catalyst were submitted to oxidation and reduction to observe the effects under XPS as shown in Figures 3.14 and 3.15. As expected, the oxidized sample produced a peak entirely positioned over the PdO region (Fig. 3.14), however the reduced catalyst produced peaks located over the metallic and native PdO regions with no indication of stoichiometric PdO present (Fig. 3.15).
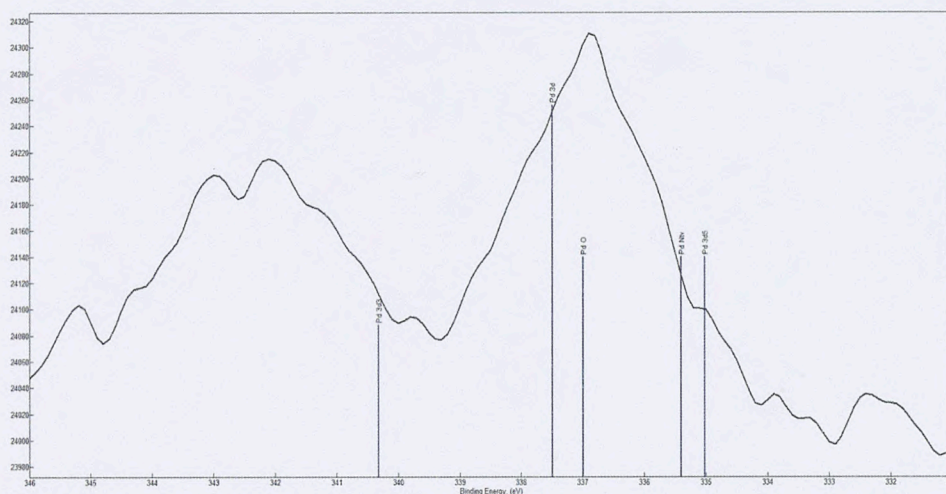

Fig. 3.14: XPS of CSU 1b. Oxidized Specimen. Pd3d$_{5/2}$ peak deconvolution
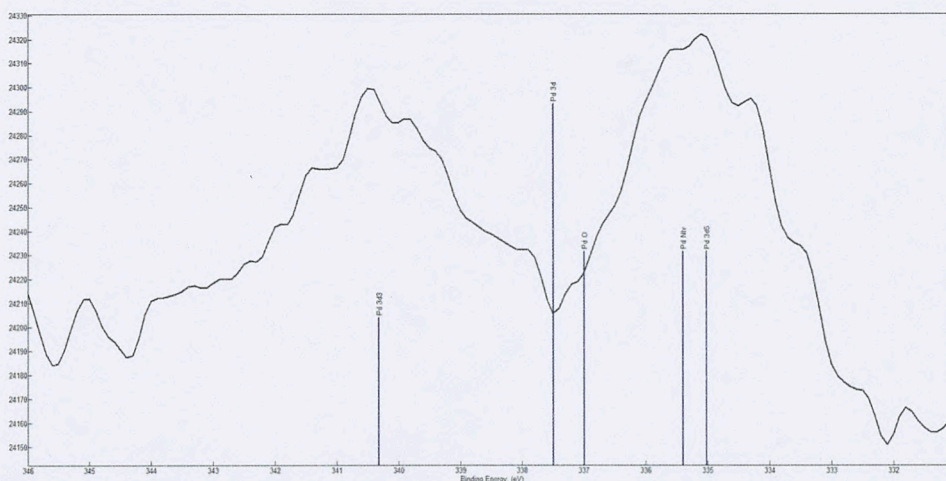

Fig. 3.15: XPS of CSU 1c. Reduced specimen. Pd3d$_{5/2}$ peak deconvolution

The purpose of submitting CSU 1 and 2 to XPS was to determine how the composition of surface species related to activity of the catalysts calcined at different temperatures. Unfortunately,

there was insufficient surface Pd within 10 nm to locate a peak on the catalyst calcined at 900 °C (CSU 2). The catalyst was sputtered to a depth of 2000Å where a peak was found over the Pd native region, which supports the same findings as sputtering on CSU 1, however it does not divulge information regarding the surface species (Figure 3.16).
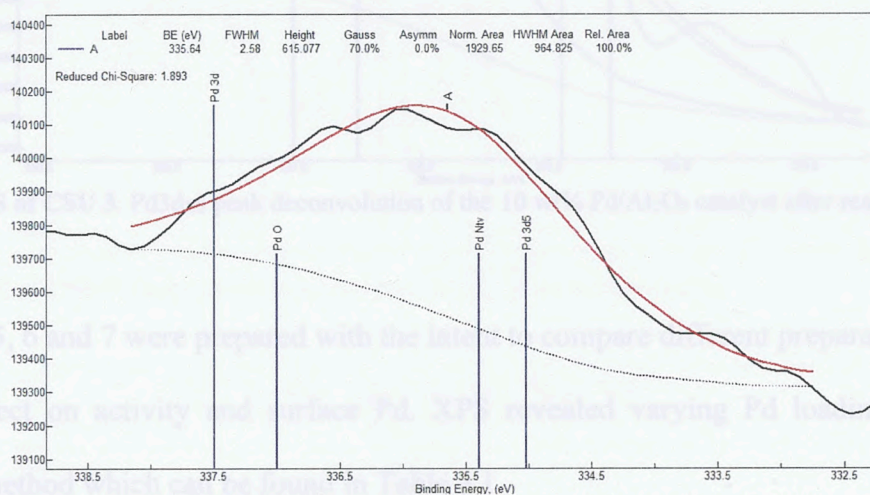

Fig. 3.16: XPS of CSU 2 - Sputtered 2000Å. 10 wt% Pd/α-Al$_2$O$_3$ calcined at 900 °C. Pd3d$_{5/2}$ peak

The purpose of sending CSU 3 for XPS was to determine the changes that occur to the surface species of the 10 wt% Pd/Al$_2$O$_3$ catalyst after catalyzing a reaction mixture of 1% CH$_4$/ 4% O$_2$. As shown in Figure 3.17, the surface PdO after reaction dropped to 52% PdO, and 48% of the surface Pd took on the phase of Pd native. Such an observation could possibly be explained by a theory that PdO converts to a species of Pd* serving as an "O-vacancy," facilitating conversion.[21] However, the species of Pd native, or non-stoichiometric Pd is undefined, where the x in PdO$_x$ could be <1 or >1. In either condition it is evident the surface reaction changes the identity of the surface Pd species.
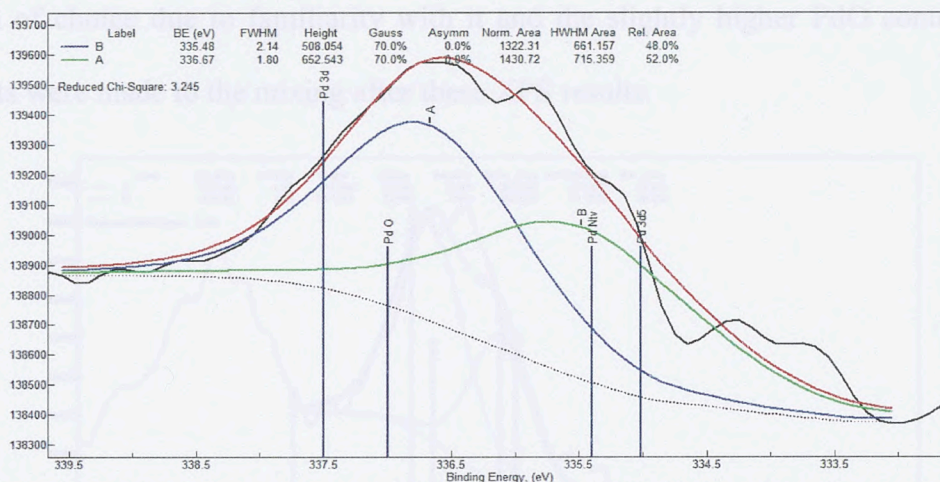
Fig. 3.17: XPS of CSU 3. Pd3d$_{5/2}$ peak deconvolution of the 10 wt% Pd/Al$_2$O$_3$ catalyst after reacting with 1% CH$_4$/ 4% O$_2$

CSU 5, 6 and 7 were prepared with the intent to compare different preparation approaches and their effect on activity and surface Pd. XPS revealed varying Pd loadings due to each preparation method which can be found in Table 3.1.

Table 3.1: Surface Pd of Various Preparation Methods

Method	Surface Pd wt%
Incipient Wetness	1.63
Wetness Impregnation	1.62
Slurry	0.54

The poor surface Pd content of the slurry method immediately ruled it out for any further use. Both impregnation techniques, incipient and wetness, were comparable in their surface Pd, however the actual surface wt% was lower than the other 10% Pd catalyst (CSU 1), adding to the doubt regarding the efficacy of the mixing procedure. The peak deconvolution of the three samples (Figures 18,19 and 20) showed the PdO:PdNtv ratio to be similar among the three methods at approximately 50:50, with the catalyst prepared by incipient wetness showing a slightly higher PdO content of 62% of total surface Pd. The incipient wetness method continued to be used as the

preparation of choice due to familiarity with it and the slightly higher PdO content, however

amendments were made to the mixing after these XPS results.

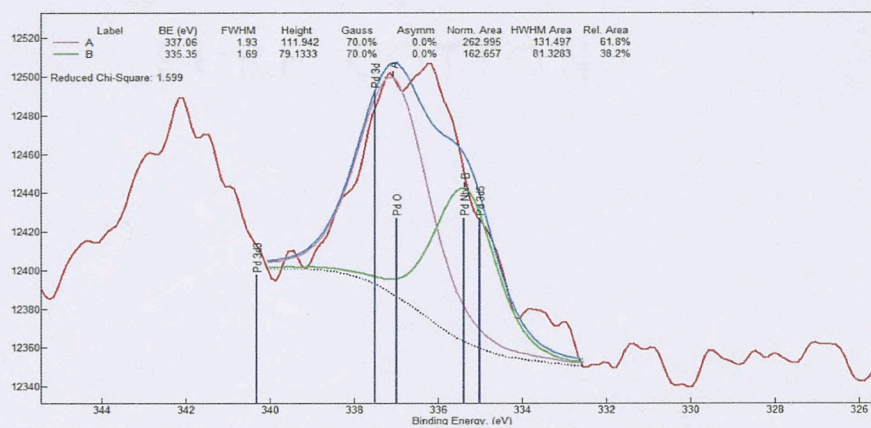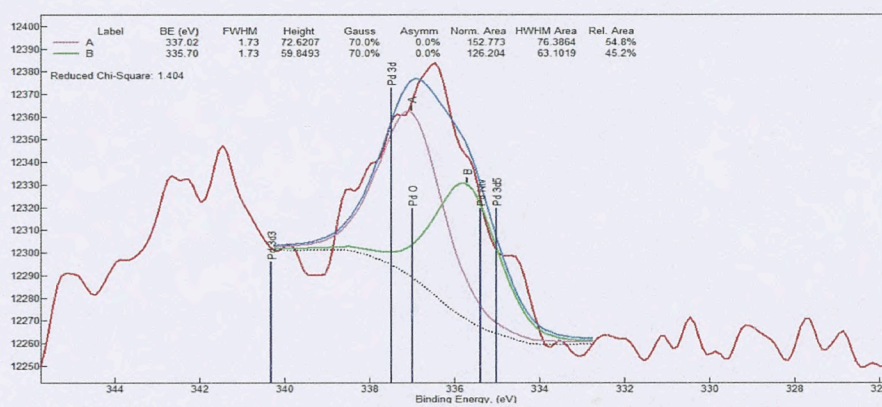**Fig. 3.18: XPS of CSU 5.** Incipient Wetness Method. Pd3d$_{5/2}$ peak deconvolution

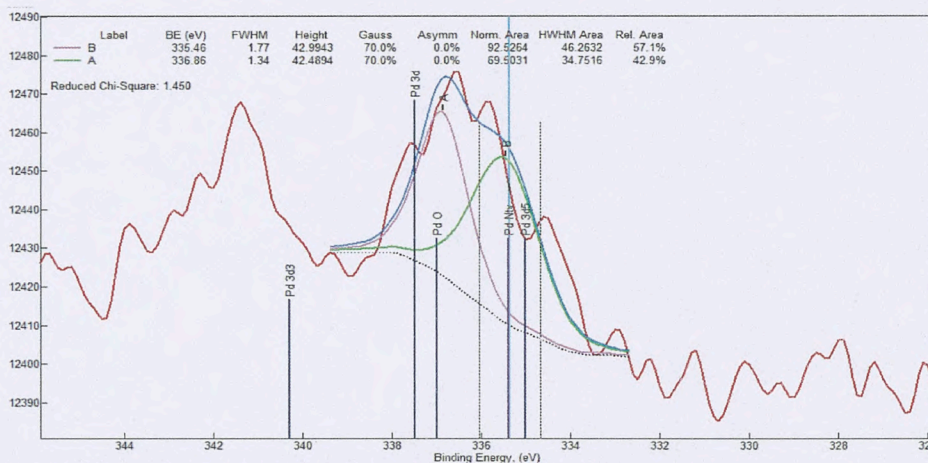**Fig. 3.19: XPS of CSU 6.** Wetness Impregnation Method. Pd3d$_{5/2}$ peak deconvolution.

Fig. 3.20: XPS of CSU 7. Slurry Method. Pd3d$_{5/2}$ peak deconvolution.

After the undesirable Pd loadings confirmed by both XPS and EDS of catalysts CSU 1-7, the preparation was amended to improve the mixing technique with a vortex mixer. The target Pd wt% was also lowered to 5 wt% to conserve the Pd precursor and the support was changed to γ-Al_2O_3 which has higher porosity.[31] The XPS of the improved catalyst 5% Pd/γ-Al_2O_3 (CSU 10) found the total surface Pd to be 1.64 wt%, which was comparable to the content of the catalyst made with twice the Pd precursor using the older mixing method and a non-specified phase of Al_2O_3. Deconvolution of the Pd3d peak of 5% Pd/γ-Al_2O_3 in Figure 3.21 shows PdO to account for 38% and Pd native 62% of the total Pd content. Activity studies would also later confirm the enhanced catalytic properties of this catalyst.
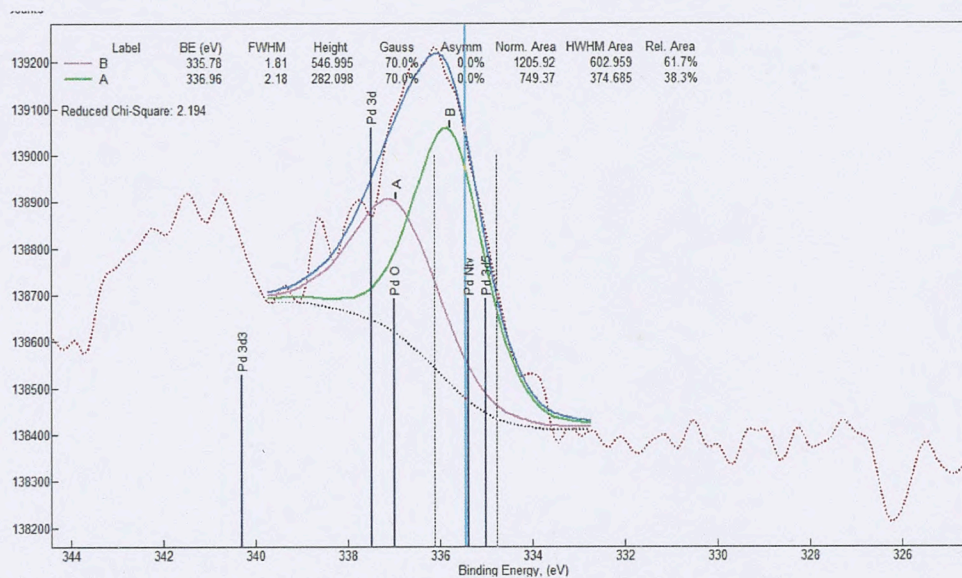
Fig. 3.21: XPS of CSU 10. Fresh 5% Pd/γ-Al_2O_3. Pd3d$_{5/2}$ peak deconvolution

After kinetics studies were performed over the 5% Pd/γ-Al_2O_3 catalyst for a duration of 80 minutes, the two used samples from combustion of 2% CH_4/ 4% O_2 and from 2% CH_4/ 8% O_2 were submitted to XPS to determine the change of phase on Pd sites due to combustion of different O_2 percentages. Figure 3.22 and 3.23 show the deconvolution of the Pd3d peaks after combustion of the two gases. After combustion of 2% CH_4/ 4% O_2, the CSU 10 catalyst showed a further shift

toward the Pd native region with the area increasing from 62% to 72% of the total Pd content, while the PdO content dropped to 28%. After CSU 10 facilitated combustion of the 2% CH_4/ 8% O_2 gas mixture, the peak shifted in the opposite direction, going from 38% PdO to 55%, and the PdNtv content dropped to 45%. To summarize, reaction with a stoichiometric mix of methane and oxygen resulted in an increase of Pd native surface species, whereas a reaction mixture containing excess oxygen resulted in an increase of PdO surface species.
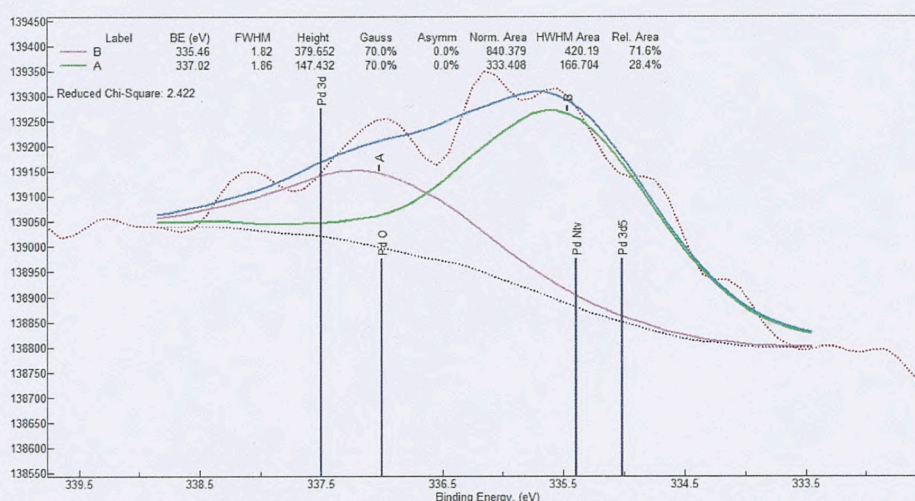

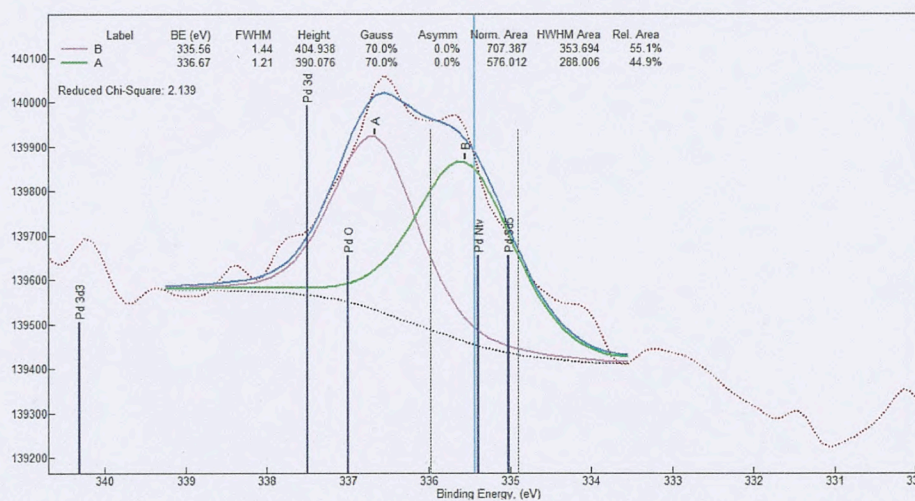**Fig. 3.22: XPS of CSU 11.** Used 5% Pd/γ-Al2O3 for combustion of 2% CH_4/ 4% O_2. Pd3d5/2 peak deconvolution

Fig. 3.23: XPS of CSU 12. Used 5% Pd/γ-Al2O3 for combustion of 2% CH_4/ 8% O_2. Pd3d5/2 peak deconvolution

As previously mentioned, the catalyst prepared as 20% Pd/γ-Al₂O₃ was made to compare the better spectroscopic resolution with catalysts of lower Pd loading, in expectation of the surface species percentages of the higher Pd loading validating the results of lower Pd loading. XPS found the 20% Pd/γ-Al₂O₃ (CSU 13) catalyst to have 4.22 wt% of Pd on the surface. Figure 3.24 shows deconvolution of the Pd3d peak of the fresh catalyst. The peak was split into 39% PdO and 61% Pd native, only a 1% difference from the results of the fresh 5% Pd catalyst. This validated the surface composition obtained from catalysts with decreased resolution due to lower Pd loadings.
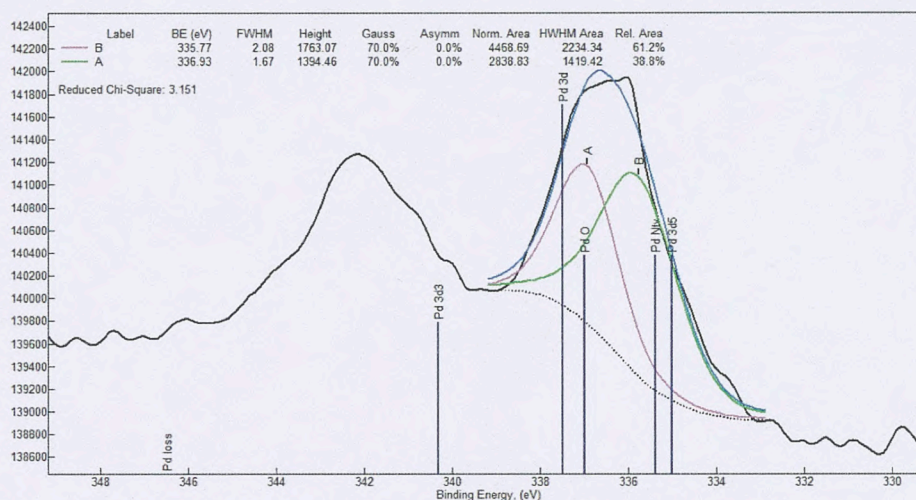
Fig. 3.24: XPS of CSU 13. Fresh 20% Pd/γ-Al₂O₃. Pd3d$_{5/2}$ peak deconvolution

When 20% Pd/γ-Al₂O₃ facilitated combustion of the 2% CH₄/ 4% O₂ gas mixture, like the 5%Pd catalyst, it caused the composition of surface Pd to shift toward formation of Pd native. However, in the case of the 20% Pd catalyst the shift was more pronounced with Pd native comprising 100% of total surface Pd after reaction. The XPS of the peak deconvolution of the catalyst after reaction is shown in Figure 3.25.
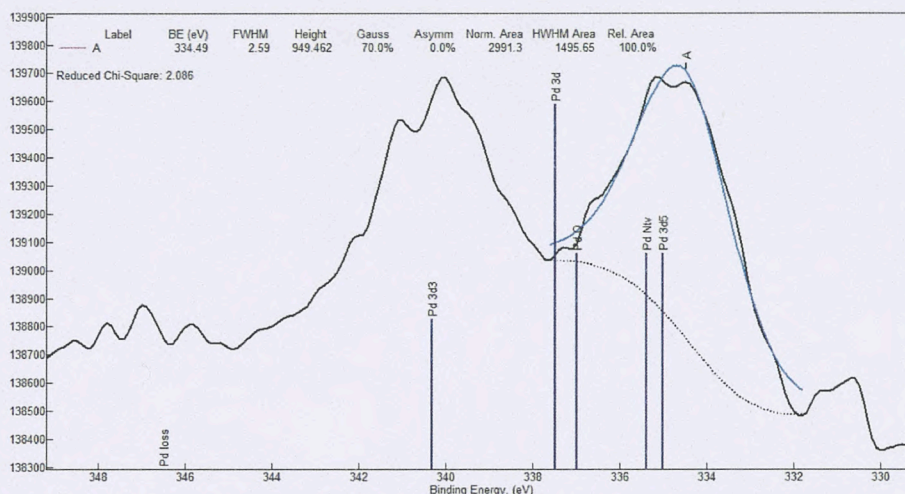
Fig. 3.25: XPS of CSU 14. Used 20% Pd/γ-Al$_2$O$_3$ for combustion of 2% CH$_4$/ 4% O$_2$. Pd3d5$_{/2}$ peak deconvolution

To ensure that the changes to the surface were indeed occurring due to reaction mixture and not by temperature effect, the 20% Pd catalyst was submitted to 80 minutes of helium flow at the same temperature as the catalyst used for reaction (280 °C). The XPS results are shown in Figure 3.26. There was a slight shift toward favoring formation of PdO with the PdO content increasing from 39% to 51% after passing helium over it. With such a slight change, the PdO increase is most likely due to experimental error, however Schwarz et al. claims that, at temperatures below 350 °C, any oxygen exchange in reaction is due to oxygen from support, so according to Schwarz, it is possible that the slight change in oxide composition could be due to some oxygen migration across the support.[23]
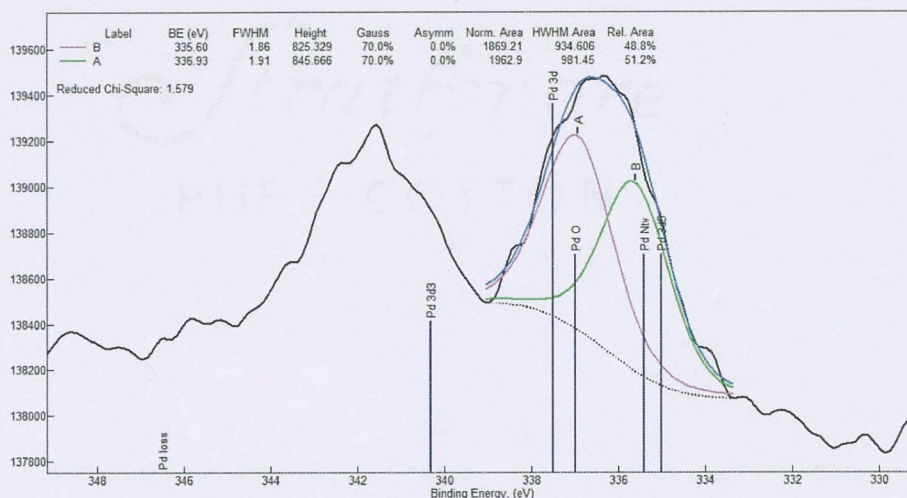
Fig. 3.26: XPS of CSU 15. Used 20% Pd/γ-Al$_2$O$_3$ for passing of helium for 80 minutes at 280 °C. Pd3d$_{5/2}$ peak deconvolution

To confirm that the observed changes to the Pd surface species after reaction were occurring due to support effects, standard grade PdO, both fresh and used for combustion of 2% CH$_4$/ 4% O$_2$, were submitted to XPS. The results for both fresh and used catalyst standard were 100% PdO, showing no change to the phase of PdO, suggesting that support played a role in the phase change. XPS of 100% PdO is shown in Figure 3.27.
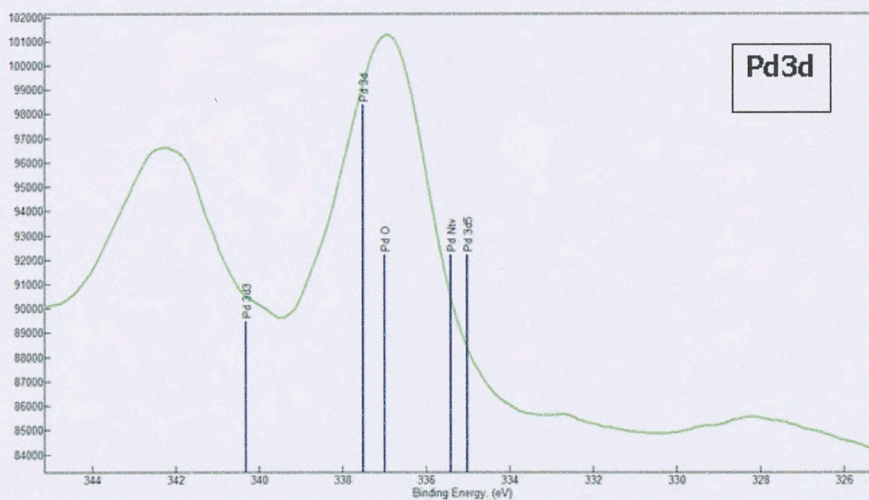
Fig. 3.27. XPS of CSU 8. Pure Standard Grade PdO. Pd3d$_{5/2}$ peak deconvolution

iv.   X-ray Diffraction

XRD analysis was performed at Auburn University to identify the Pd compounds comprising the bulk of the catalyst, not just surface species as in XPS. For comparison purposes, pure γ-Al_2O_3, and pure standard grade PdO were analyzed to identify peaks of interest in the catalysts CSU 10 and CSU 13. The XRD results are shown in Figures 3.28 and 3.29. The important peaks arising from the alumina support are the peaks at 46.0° and 67.4° and the identifying peaks for PdO are a strong peak at 34.1° and lesser peaks at 42.2°, 54.9°, 61.1°, and 71.7°.
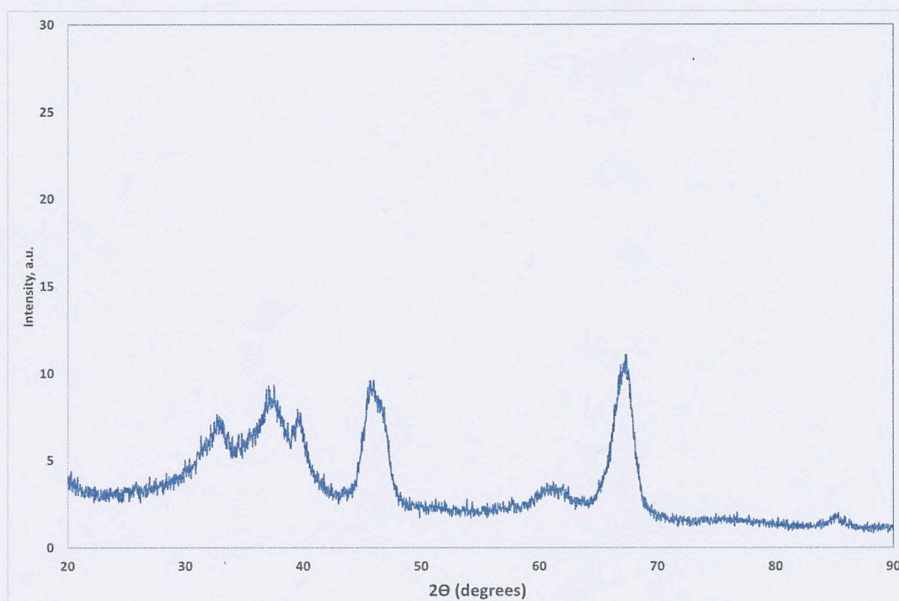
Fig. 3.28: XRD of γ-Al_2O_3.
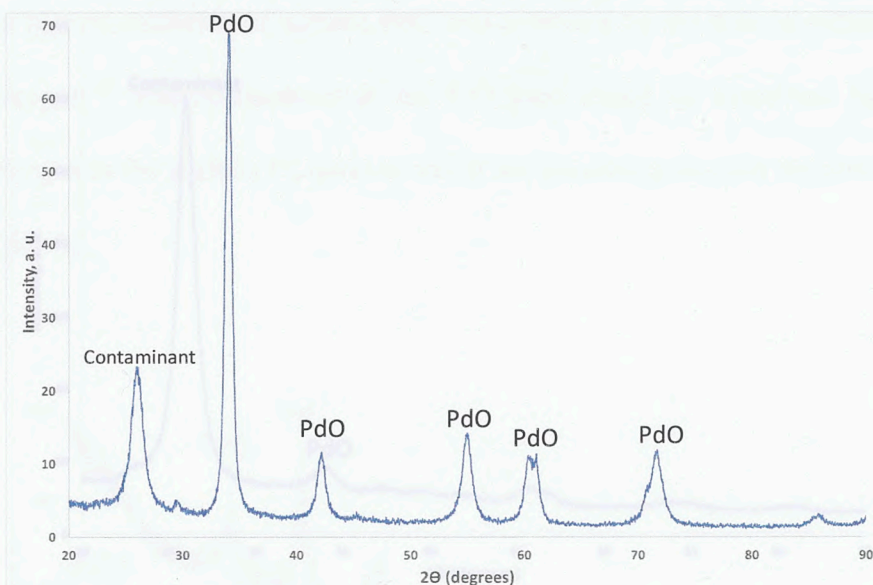
Fig. 3.29. XRD of Standard Grade PdO

The XRD analysis of the 5% Pd/γ-Al$_2$O$_3$ (CSU 10) catalyst, as expected, had low resolution

of peaks due to low Pd loadings. However, a peak can be detected at 33.8° which is the location

of the characteristic strongest line for PdO, as found in the XRD of pure PdO and as published by

other researchers.[27, 40-41] An unexpected outcome of the 5% Pd/γ-Al$_2$O$_3$ XRD is the strong peak at

26.0°. While a moderate peak in that range appeared in the XRD for pure PdO in Figure 3.29, it is

not a PdO peak found in the ICDD nor is it documented by other researchers identifying PdO via

XRD, which caused suspicion that it might be due to a contaminant species. Lin et al. found a peak

in the same location on their XRD of Pd on graphene, which was attributed to carbon.[41]

Considering the XPS data also contains contamination by atmospheric carbon (see Figure 3.10), it

is plausible that the 26.0° peak was carbon. Also, double-sided tape was used in preparing the

samples for XRD and that could also be a possible origin of the unexpected peak.
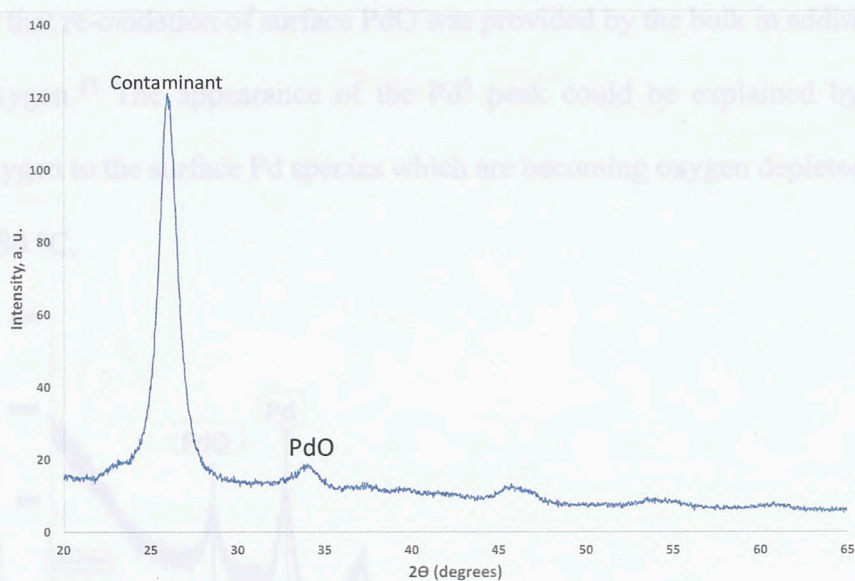
Fig. 3.30: XRD of CSU 10. 5%Pd/γ-Al$_2$O$_3$

A higher resolution XRD was demonstrated by the 20% Pd/γAl$_2$O$_3$ catalyst, as well as a comparison of fresh catalyst to the catalyst after reaction with 2% CH$_4$/ 4% O$_2$ in Figure 3.31. The lower redline corresponds to the fresh catalyst and the upper blue line corresponds to the used catalyst. Both catalysts displayed the characteristic strong PdO peak at 34°, as well as some of the lesser PdO peaks, however all PdO peaks are more pronounced in the fresh catalyst. Of interest, is the sharp peak at 40° and a lesser peak at 81° displayed in the used catalyst that are not present in the fresh catalyst. These peaks have been cited by other authors as Pd^0 peaks or metallic Pd.[41-42] Also, all of the PdO peaks in the used catalyst decreased in intensity suggesting a decrease in its concentration. Keeping in mind that XRD is a bulk spectroscopic technique, this data could elucidate the fluctuation between PdO and PdO$_x$ that was observed on the surface of the catalyst. According to Schwartz et al., oxygen exchange involving gas-phase oxygen is negligible at temperatures below 350 °C, which is the range in which the used catalyst operated. Schwartz instead concludes that oxygen for reaction at these lower temperatures is significantly provided by oxygen bonded to Pd.[23] These conclusions were formed based off previous work by Ciuparu et al.,

who concluded that re-oxidation of surface PdO was provided by the bulk in addition to gas-phase and support oxygen.[45] The appearance of the Pd^0 peak could be explained by the bulk PdO contributing oxygen to the surface Pd species which are becoming oxygen depleted as the reaction progresses at 280 °C.
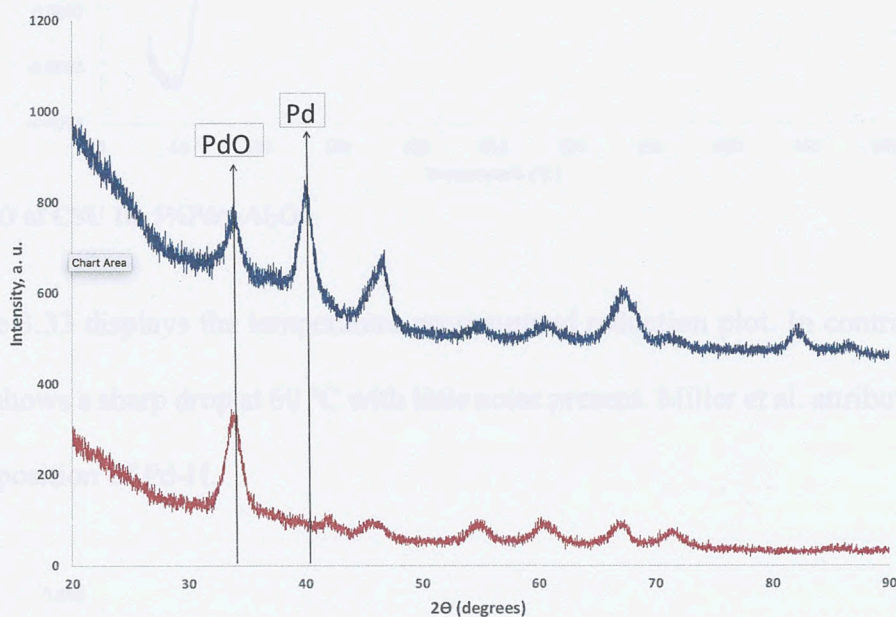
Fig. 3.31: XRD of CSU 10. Fresh 20%Pd/γ-Al₂O₃ is shown in the lower red line. Used 20%Pd/γ-Al₂O₃ is in the top blue.

v.   TPO/TPR

Temperature programmed oxidation of the 5% Pd/γ-Al₂O₃ catalyst is shown in Figure 3.32. The plot is noisy, displaying no definitive oxygen uptake. Miller et al. discusses the important temperature for TPO studies of Pd/Al₂O₃ as being around 286 °C where the Pd to PdO transition occurs.[21] A noisy rise between 250-300 °C on the plot in Figure 3.32 could possibly be representative of oxygen uptake as Pd transitions to PdO. However, the rise is subtle and lacking definition. The more likely explanation of the plot's noise is that the sample already had high content of PdO prior to the oxidation procedure, as neither XRD nor XPS found metallic Pd present in the fresh 5% Pd/γ-Al₂O₃ catalyst.
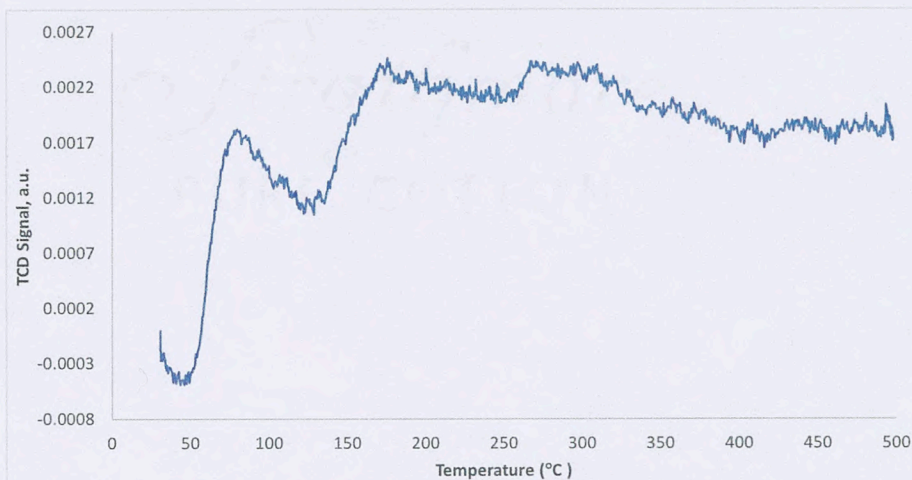
Fig. 3.32: TPO of CSU 10. 5%Pd/γ-Al₂O₃

Figure 3.33 displays the temperature programmed reduction plot. In contrast to the TPO results, TPR shows a sharp drop at 60 °C with little noise present. Miller et al. attributes this marker as the decomposition of Pd-H.
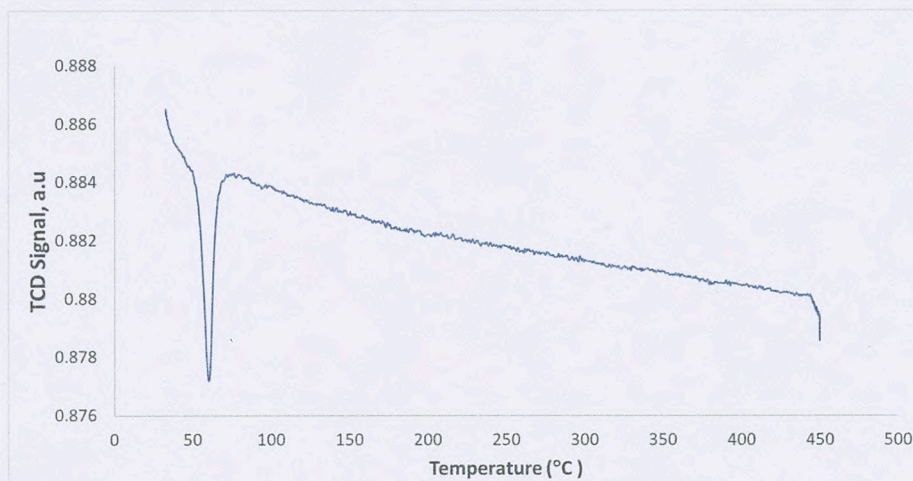
Fig. 3.33: TPR of CSU 10. 5%Pd/γ-Al₂O₃

vi.   N₂ physisorption

Physisorption results provided information regarding the surface area of the 5% Pd/γ-Al₂O₃ catalyst. Of importance, is the Brunauer-Emmett-Teller (BET) surface area. This divulged the catalyst's monolayer capacity, which is the amount of adsorbate needed to cover 1 gram of the

solid.[14] For the 5% Pd/γ-Al$_2$O$_3$ catalyst, the BET value is 148 m^2/g. This value is about a third of the surface area described by Schwarz et al. with a similar 3 wt% Pd/Al$_2$O$_3$ catalyst.[23]

vii.   CO Chemisorption

CO chemisorption with reduction showed a 56.193 μmol/g uptake, which yields an 11.95% dispersion (amount of Pd atoms at surfaces of crystallites), and a metal surface area of 2.66 m^2/g. The Pd particle size was found to be 9.37 nm, which is smaller than what Schwarz et al. reported with a 12 nm particle diameter, but larger than the Pd particles produced by Miller et al., which ranged 3.6-5.3 nm for Pd on alumina support. It has been suggested the choice of Pd precursor plays a role in the Pd particle size.[21] Schwartz used a nitrate dihydrate precursor[23] and Miller used nitrate and tetraamine precursors.[21] CO chemisorption without reduction showed a significantly decreased uptake at 17.69 μmol/g, which could be expected considering that, without reduction, some sites remained as PdO, potentially inhibiting the CO uptake. Other researchers previously mentioned did not report using the CO without reduction method.

viii.   Activity

Figure 3.34 displays activities of CSU 1, 1a, and 2, which were 10 wt% Pd/α-Al$_2$O$_3$ catalysts calcined at 600, 750 and 900 °C respectively. The best performing catalyst was calcined at 600 °C, initiating catalysis at 310 °C and reaching a maximum of 98%conversion at 392 °C. The two catalysts calcined at 750 °C and 900 °C initiated catalysis <300 °C, but never achieved >80% conversion below 400 °C, which was the targeted range for this study. PdO has been cited as remaining stable up to 800 °C, therefore it was expected that higher calcined catalysts would exhibit higher amounts of metallic Pd, which could have had effect on activity.[13] Supported Pd catalysts are also reported as exhibiting poor dispersion at higher temperatures.[12] The decreased

dispersion could be attributed to sintering in which the Pd particles migrate and agglomerate into larger particles irreversibly starting at temperatures as low as 570 °C.[22, 46] XPS revealed the 600 °C calcined catalyst as having all of its surface Pd in the form of PdO, which confirmed the catalytic activity of the PdO phase. XPS was unable to detect sufficient amount of Pd on the surface of the 900 °C calcined catalyst. Given the calcination temperature above the threshold for sintering, it could be suggested that the decreased surface Pd was a result of decreased dispersion due to sintering. This would explain the lower catalytic activity as well. XPS was not conducted on the fresh 750 °C calcined catalyst, however a decreased activity coinciding with high calcination temperature could be a result of sintering as with the 900 °C calcined catalyst. More recent publications on supported Pd catalysts report effective calcination temperature in the range of 400-500 °C, thus all catalysts prepared after CSU 2 were calcined at 500 °C to encourage PdO formation and prevent sintering.[21, 23, 29]

Fig 3.34: Conversion vs. Temperature – Varying Calcination Temperatures

Figure 3.35 displays CSU 9 and 10 which were both prepared by vortex incipient wetness as 5 wt% Pd/γ-Al$_2$O$_3$ differing in preparation only by the Pd precursor. CSU 9 was prepared with a dihydrate precursor, and CSU 10 was prepared using a hydrate precursor. While the decision to abandon use of the dihydrate was originally made in an effort to remain consistent with precursors, activity confirms the decision because the nitrate hydrate both initiated conversion earlier, <275 °C, and also achieved near complete conversion of 94% at 325 °C, both of which outperform CSU 9. This could be due to CSU 10 having a smaller particle size than CSU 9. Schwarz et al. reported obtaining a 12 nm particle using a nitrate dihydrate precursor as used for CSU 9, but Miller et al. produced particles ranging 3.6-5.3 nm using nitrate hydrate and tetraamine precursors.[21] The particle size for CSU 9 was not measured, but the particle size for CSU 10 was found to be 9.37 nm which is smaller than the particle size reported by Miller using a nitrate dihydrate precursor.
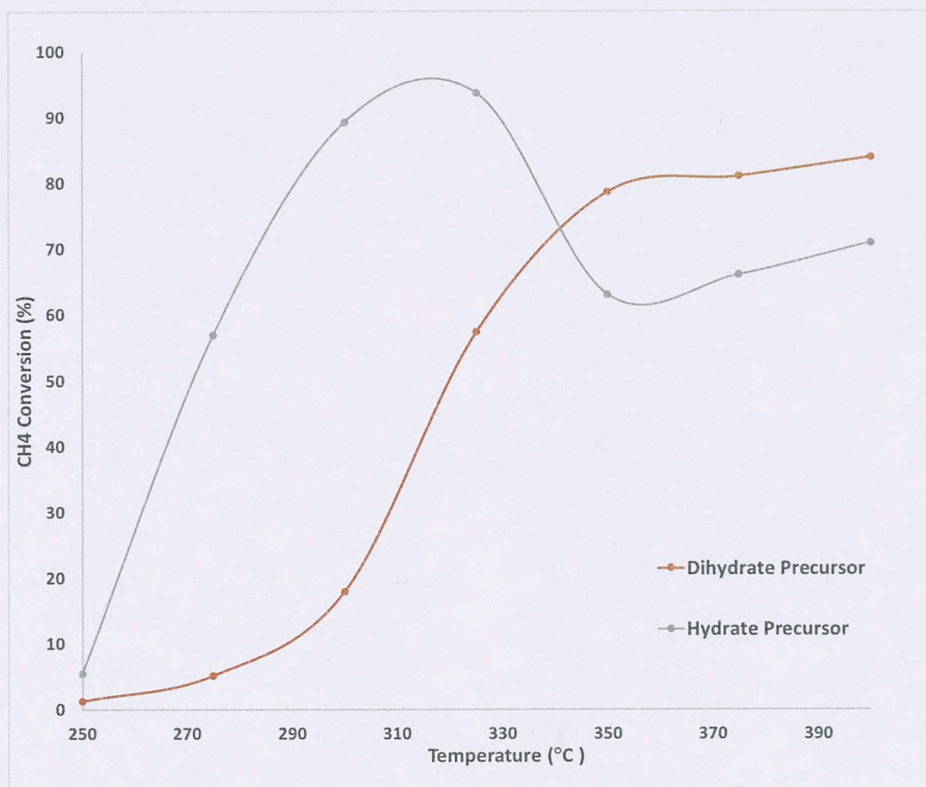
Fig. 3.35: Conversion vs. Temperature -Varying Pd Precursors. 5% Pd catalysts prepared using palladium nitrate dihydrate and palladium nitrate hydrate precursors

Figure 3.36 displays the catalysts which exhibited the highest activity and were submitted for the most extensive characterization. Thus, these three catalysts provide the most information regarding the Pd phase and catalytic activity relationship. CSU 8, represented by the blue line in Figure 3.36, was the unsupported standard PdO catalyst obtained from Sigma Aldrich. As anticipated, 0.200 g of the standard initiated combustion and achieved 100% conversion at the lowest observed temperature <250 °C. Interestingly, while initiation was not as low as the 100% PdO, the 20 wt% Pd/γ-Al$_2$O$_3$ (CSU 13) also achieved a 100% conversion at 250 °C utilizing a fraction of the palladium present in the standard. Of specific interest, the 5 wt% Pd/γ-Al$_2$O$_3$ initiated combustion at 250 °C and achieved a peak 94% conversion at 325 °C with the lowest Pd loading of the three highly active catalysts. Kinetics performed on this 5 wt% Pd/γ-Al$_2$O$_3$ catalyst would provide more clarity regarding the surface reaction.
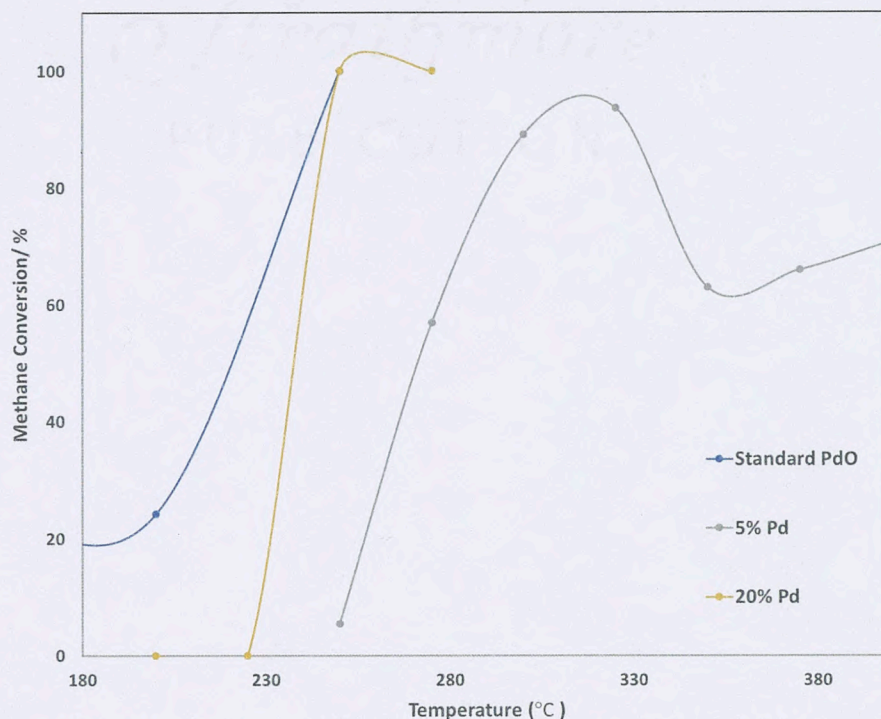
Fig. 3.36: Conversion vs. Temperature – Highest Activity Catalysts. 5% Pd and 20% Pd catalysts compared to pure standard grade PdO

ix.   Kinetics

A fixed temperature of 280 °C was chosen to study the effect methane and oxygen concentrations have on conversion over time, because this temperature fell in between catalyst activation and full conversion. Figure 3.37 shows how conversion changed over time for a mixture of 1% CH_4/ 4%O_2/ balance He and a mixture of 2% CH_4/ 4%O_2/ balance He. The 1% CH_4 mixture took 20 minutes to achieve a peak conversion of 56%. After that point, % conversion showed a steady decline. The 2% CH_4 mixture showed a sharper increase in conversion and peaked at 5 minutes into reaction with a 92% conversion. Like the 1% mixture, the 2% CH_4 experienced a steady decline in activity after reaching peak conversion. The rate of increasing conversion in the early minutes of reaction showed significant change dependent on the CH_4 concentration, and the

declining conversion also showed a steeper slope for the higher methane concentration. This implied that concentration of methane affected the reaction mechanism.
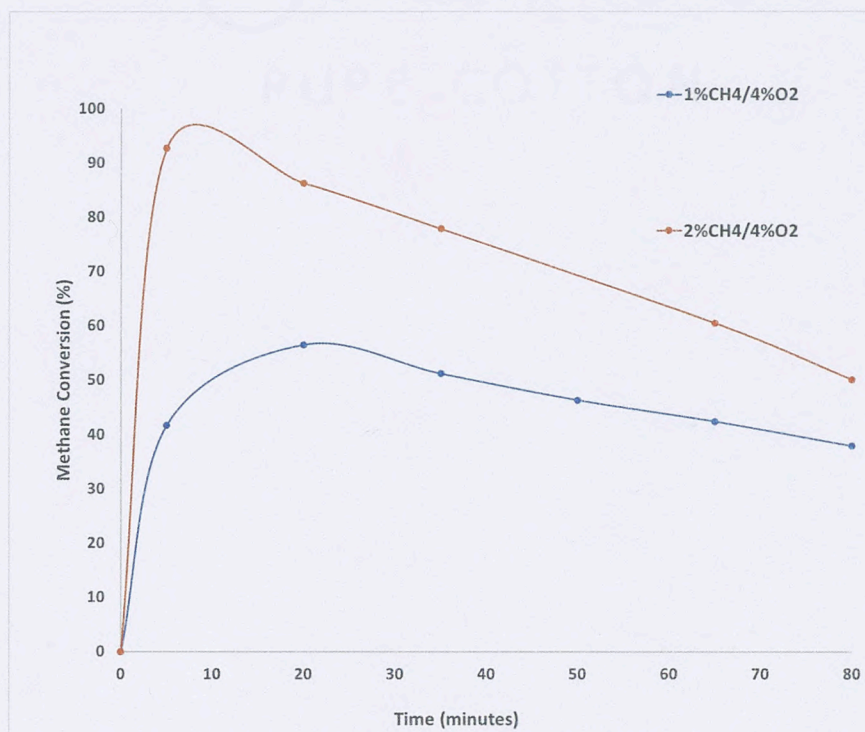
Fig. 3.37: Conversion vs. Time – Varying Methane Concentration. Kinetics on 5%Pd/γ-Al$_2$O$_3$, comparing 1% and 2% CH$_4$ reaction mixtures, O$_2$ held constant

Figure 3.38 shows how conversion changed over time for a mixture of 2% CH$_4$/ 4%O$_2$/ balance He and a mixture of 2% CH$_4$/ 8%O$_2$/ balance He. In this comparison, the methane concentration was held constant, but the O$_2$ concentration was doubled. Both reaction mixtures achieved peak conversion within the first 5 minutes of reaction, with the 4% O$_2$ mix reaching 92% conversion and the 8% O$_2$ mixture peaking at 84% conversion. The rates of increasing conversion appeared to be similar, as well as the rate for declining conversion, implying that concentration of O$_2$ had little to no effect on the rate of reaction. Further rate calculations would provide more specific details regarding the mechanistic dependency on gas concentrations.
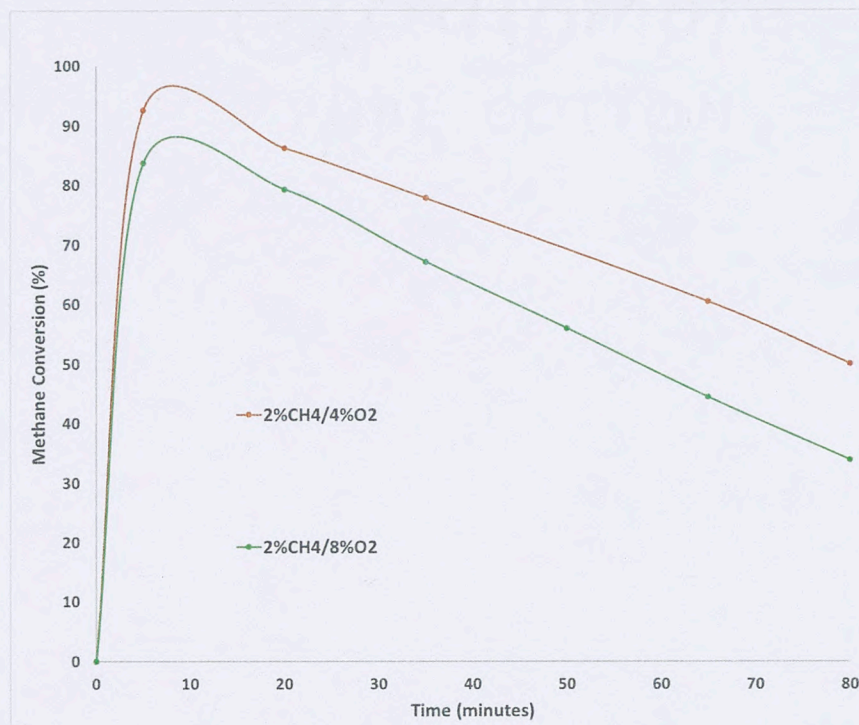
Fig. 3.38: Conversion vs. Time – Varying Oxygen Concentration. Kinetics on $5\%Pd/\gamma-Al_2O_3$, comparing 4% and 8% O_2 reaction mixtures, CH_4 held constant

B. Discussion

Percent Conversion for the activity and kinetics studies was calculated using the following equation:

$$\%Conversion = \frac{[mol\ CH_4]_{in} - [mol\ CH_4]_{out}}{[mol\ CH_4]_{in}} \times 100\%$$

For every sample of reacted gas mixture, the corresponding peak area from the GC was translated into % conversion and entered into the graphs found in Figures 3.37 and 3.38. From the % conversion, a rate in $\mu mol \cdot gPd^{-1} \cdot s^{-1}$ was calculated for a given reaction duration. An example of the rate calculation is demonstrated in the following rate for $1\%CH_4/ 4\%\ O_2$ after 5 minutes of reaction:

For 1% methane:

$$\frac{1mL\ CH_4}{100mL\ gas} \times \frac{1000mL}{min} \times 5\ min$$

$$= 50mL\ CH_4\ sent\ to\ reactor\ over\ 5\ minutes$$

$$n = \frac{PV}{RT} = \frac{(1.0atm)(0.05L)}{(0.0821\frac{atm \cdot L}{mol \cdot K})(298K)} = 2.04 \times 10^{-3}\ [CH_4]_{in}$$

At 5 minutes sampled gas contained 0.58% methane

$$\frac{0.58mL}{100mL} \times \frac{1000mL}{min} \times 5\ min = 29mL\ CH_4$$

$$n = \frac{PV}{RT} = \frac{(1.0atm)(0.029L)}{(0.0821\frac{atm \cdot L}{mol \cdot K})(298K)} = 1.19 \times 10^{-3}\ [CH_4]_{out}$$

Moles converted:

$$2.04 \times 10^{-3} mol\ CH_{4\ in} - 1.19 \times 10^{-3}\ mol\ CH_{4\ out}$$

$$= 0.85 \times 10^{-3} mol\ CH_4\ converted\ to\ product$$

% Conversion:

$$\%Conversion = \frac{[mol\ CH_4]_{in} - [mol\ CH_4]_{out}}{[mol\ CH_4]_{in}} \times 100\%$$

$$\frac{0.85 \times 10^{-3}\ mol\ CH_4}{2.04 \times 10^{-3}\ mol\ CH_{4\ in}} \times 100 = 42\%\ conversion$$

$$= \frac{42\ moles\ of\ CH_4\ converted}{100\ moles\ of\ CH_4\ fed}$$

Rate for 1% CH$_4$:

$$rate = \frac{\mu mol\ CH_4\ converted}{(gram\ surface\ Pd)(reaction\ time, s)}$$

$$gram\ surface\ Pd = 1.64\%\ surface\ Pd \times 0.2g\ catalyst\ in\ reactor = 3.28 \times 10^{-3} g\ Pd$$

$$reaction\ time = 5min \times \frac{60\ s}{min} = 300\ s$$

$$r_1 = \frac{8.5 \times 10^2 \mu mol\ CH_4\ converted}{(3.28 \times 10^{-3}g\ Pd)(300\ s)} = 864\ \mu mol \cdot gPd^{-1} \cdot s^{-1}$$

In the same manner, rates were determined for each of the three reaction mixtures at 5 minutes and at 20 minutes. Those rates are listed in Table 3.2.

Table 3.2: Rates of reaction for 3 different gas mixtures at 5 and 20 minutes

CH$_4$	O$_2$	Reaction Time = 5 Minutes	Reaction Time = 20 Minutes
1%	4%	$r_1 = 864\ \mu mol \cdot gPd^{-1} \cdot s^{-1}$	$r_1 = 4644\ \mu mol \cdot gPd^{-1} \cdot s^{-1}$
2%	4%	$r_2 = 3,834\ \mu mol \cdot gPd^{-1} \cdot s^{-1}$	$r_2 = 14,228\ \mu mol \cdot gPd^{-1} \cdot s^{-1}$
2%	8%	$r_3 = 3,465\ \mu mol \cdot gPd^{-1} \cdot s^{-1}$	$r_3 = 13,211\ \mu mol \cdot gPd^{-1} \cdot s^{-1}$

The kinetic runs had limitations with only two sets of concentrations for each reactant. While quantitative conclusions need more data, some qualitative conclusions can be drawn from Table 3.2. The data for 20 minutes of reaction were more reliable since the runs after 5 minutes may have had more sampling errors. The rate of reaction increased three-fold when the methane concentration doubled at constant oxygen concentration. However, when oxygen concentration doubled, there was virtually no change in the rate. While the order is not calculated, it is apparent that the concentration of methane in the gas mixture drives the rate of reaction and that the oxygen concentration has no influence, as a zero-order reaction might behave. This observation rules out the likelihood of a Langmuir-Hinshelwood (L-H) mechanism, as the L-H model requires both reactants to adsorb to the surface of the catalyst and participate in the reaction. Eley-Rideal mechanism is a possibility, with methane in the gas phase reacting with adsorbed oxygen molecules on the surface. The preliminary kinetics runs suggest the rate to be increasing with

increasing concentration of methane and the rate being almost independent of oxygen concentration. Such preliminary observations support Eley-Rideal mechanism.

In order to discuss the mechanistic details any further, there were several observations regarding migration of oxygen that need to be reiterated. Firstly, a freshly prepared Pd/γ-Al_2O_3 catalyst contains a mixture of PdO and PdNtv, but post-reaction PdO content decreases in both the bulk and the surface, while PdNtv content increases on the surface and metallic Pd^0 develops in the bulk. Secondly, unsupported, standard grade PdO facilitates complete combustion of methane, and post-reaction, maintains 100% PdO content, with no presence of PdNtv oxide. The evidence from XPS clearly show that in the absence of the support, PdO is the stable and active phase before and after reaction in the catalytic oxidation of methane. Thirdly, XPS data also clearly show that the support, γ-Al_2O_3, plays a significant role in changing the surface composition and converts PdO to Pd native oxides in the calcination process. One possible reason could be oxide ions from the support migrate to PdO and convert it to Pd native oxides. Another, explanation could be oxygen transfer between PdO and PdNtv. Therefore, it seems both PdO and Pd native oxides are the active phases in the presence of the support. XPS of 20% Pd/γ-Al_2O_3 after reaction with $2\%CH_4/4\%O_2$ reveal the presence of 100% Pd native oxide and no PdO. This cannot be explained alone by the support effect. It may be possible that during the reaction the adsorbed oxygen molecules on the surface reacted with PdO to form Pd native oxide.

The Eley-Rideal mechanism alone could not explain the disappearance of surface and bulk PdO, indicating the possibility that a more complex mechanism is occurring. It appears that some oxygen for the combustion of methane is being contributed by the bulk in a Mars-van-Krevlen type mechanism as described in the work by Fujimoto et al.,[47] and the rest of the oxygen to complete the combustion is being provided in an Eley-Rideal type mechanism by the adsorbed

oxygen. However, the limited kinetics data retrieved by this study are insufficient to propose any further conclusion regarding specific mechanisms. A more detailed kinetic study involving different partial pressures of methane and oxygen would provide better insights into the mechanism.

Thus, the results of this research are consistent with the works of Miller and Schwartz,[21,23] highlighting the roles of PdO and PdNtv in the combustion of methane at low-temperatures, and corroborating that alumina as a support material helps stabilize the PdNtv species and facilitates oxygen migration.

IV. CONCLUSIONS AND FUTURE WORK

A. Conclusions

In regard to catalyzing methane, palladium has been the element of choice in recent years, even though the mechanism of its action is still not fully understood. What is known, however, is that palladium is the best performer at low temperatures which are typical of lean-burn conditions.[12] To date, an ideal catalyst that performs optimally under 400 °C is undiscovered, but palladium, supported on various materials comes close, as it has been shown to initiate oxidation at 400 °C.[5] One of the major objectives of this current research was to develop a catalyst that will oxidize methane at a low temperature below 400 °C. Based on the initial trials and screening with a variety of alumina supported palladium catalysts, an improved vortex-assisted incipient wetness method was finally developed to prepare a catalyst having higher Pd content on the surface. A 5 wt% $Pd/\gamma-Al_2O_3$ was prepared by this method and calcined at 500 °C. This catalyst converted 94% (mol/mol) methane at 325 °C and was found to be a better catalyst for low-temperature combustion of methane than recently published Pd/ZrCe, PdCe, and bi-metallic $Pt-PdAl_2O_3$.[21, 26]

The second objective of this study was to characterize the surface compounds present on the surface of the catalysts before and after reaction. Identification of compounds (metallic Pd, PdO, PdNtv oxides, and $\gamma-Al_2O_3$) present on the surface of the catalysts (within 10 nm) was mainly done through X-ray Photoelectron Spectroscopy (XPS). In the absence of the support, the surface contained PdO, PdNtv oxides and $\gamma-Al_2O_3$ and no metallic Pd. The surface composition did not alter after reaction with methane and oxygen for the unsupported catalysts. The evidence from XPS confirmed PdO was the active and stable phase before and after the reaction, and no palladium native oxide (PdNtv) was found on the surface. However, in the presence of the support, gamma-aluminum oxide, the surface composition changed substantially. The surface had PdO, PdNtv oxide and $\gamma-Al_2O_3$ as confirmed by XPS data. The atmospheric oxygen during the calcination

process did not change the standard PdO to PdNtv oxide. Thus, it appears that PdNtv oxide, a non-stoichiometric palladium oxide Pd_xO_y in the alumina supported catalysts, originated from migration of oxide ions to stoichiometric PdO on the surface. It appears both PdO and PdNtv oxide were active species in the catalytic oxidation in the presence of γ-Al_2O_3 as a support. The depletion of PdO and increase in PdNtv oxide percentage were also observed in the XPS spectra of the catalysts after reaction with methane and oxygen. This suggests the support could facilitate oxygen mobility and affect composition of the surface catalytic sites at temperatures <400 °C. This observation corroborates the research findings of Miller et al. and Schwartz et al.[21, 23]

The final objective of the study was to suggest a reaction mechanism for the surface reaction based on XPS and preliminary kinetic data. The preliminary kinetic runs suggested the rate to be increasing with increasing concentration of methane and the rate being almost independent of oxygen concentration. These preliminary observations infer a bimolecular surface reaction following Eley-Rideal mechanism. In this mechanism, oxygen would be adsorbed on the catalytic surface and methane would be in the gas phase, followed by a surface reaction between adsorbed oxygen molecules and gas phase methane molecules as the rate determining step. The catalyst surface composition changed to 100% PdNtv oxide and 0% PdO after reaction with 2% methane and 4% oxygen. A probable explanation could be the adsorbed oxygen molecules on the surface reacted with PdO to form Pd native oxide (Pd_xO_y; x<y).

B. Future Work

In order to elucidate the catalytic mechanism, more extensive work on kinetics needs be conducted. This would require more studies on the effects of partial pressures of methane and oxygen on the rate of the reaction. Other areas of future research would include determination of thermal stability and the turn over number (TON) of the catalyst, and the issue of catalyst deactivation by water and/or other substances.[11, 21, 26, 35-36]

V. BIBLIOGRAPHY

1. *Inventory of U.S. Greenhouse Gases and Sinks, 1990-2015*; U.S. Environmental Protection Agency. U.S. Government Printing Office: Washington, D.C., 2017

2. Friedman, L. Court Blocks E.P.A. Effort to Suspend Obama-Era Methane Rule. *The New York Times*. July 3, 2017. https://nyti.ms/2uDCpZI

3. Controlling Air Pollution from the Oil and Natural Gas Industry. https://www.epa.gov/controlling-air-pollution-oil-and-natural-gas-industry/actions-and-notices-about-oil-and-natural-gas#regactions (accessed March 4, 2017)

4. Cama, T. Court: Trump Admin Must Enforce Obama Methane Leak Rule. *The Hill*. February 28, 2018. http://thehill.com/policy/energy-environment/375225-court-trump-admin-must-enforce-obama-methane-leak-rule-for-oil-and

5. Farrauto, R. J. (2012). Low-Temperature Oxidation of Methane. *Science*, *337*(August), 659–660.

6. *Methane*. CDC. International Chemical Safety Cards: 0291. (2000).

7. Höglund-Isaksson, L. (2012). Global anthropogenic methane emissions 2005-2030: Technical mitigation potentials and costs. *Atmospheric Chemistry and Physics*, *12*(19), 9079–9096. http://doi.org/10.5194/acp-12-9079-2012

8. Turner, A. J., Jacob, D. J., Wecht, K. J., Maasakkers, J. D., Lundgren, E., Andrews, A. E., … Wunch, D. (2015). Estimating global and North American methane emissions with high spatial resolution using GOSAT satellite data. *Atmospheric Chemistry and Physics*, *15*(12), 7049–7069. http://doi.org/10.5194/acp-15-7049-2015

9. Allen, D. T. (2014). Methane emissions from natural gas production and use: Reconciling bottom-up and top-down measurements. *Current Opinion in Chemical Engineering*, *5*, 78–83. http://doi.org/10.1016/j.coche.2014.05.004

10. Environmental Protection Agency. (2017). EPA and NHTSA Set Standards to Reduce Greenhouse Gases and Improve Fuel Economy for Model Years 2017-2025 Cars and Light Trucks, (August 2012).

11. Cargnello, M., Delgado Jaen, J., Bakhmutsky, K., Montini, T., Calvino Gamez, J., Gorte, R., Fornasiero, P. (2012). Exceptional Activity for Methane Combustion over Modular Pd@CeO2 Subunits on Functionalized Al2O3. *Science*, *337*(August), 713–717.

12. Gélin, P., & Primet, M. (2002). Complete oxidation of methane at low temperature over noble metal based catalysts: a review. *Applied Catalysis B: Environmental*, *39*(1), 1-37.

13. Bychkov, V. Y., Tyulenin, Y. P., Gorenberg, A. Y., Sokolov, S., & Korchak, V. N. (2014). Evolution of Pd catalyst structure and activity during catalytic oxidation of methane and ethane. *Applied Catalysis A: General, 485*, 1-9.

14. Rothenberg, G. (2017). *Catalysis: concepts and green applications*. John Wiley & Sons.

15. Kinnunen, N. M., Hirvi, J. T., Venäläinen, T., Suvanto, M., & Pakkanen, T. A. (2011). Procedure to tailor activity of methane combustion catalyst: Relation between Pd/PdOx active sites and methane oxidation activity. *Applied Catalysis A: General, 397*(1-2), 54-61.

16. Overman, L. (2003). Palladium. *C & EN*, September, 2003. http://www.cen-online.org

17. Cotton, F. Albert; Gaus, Paul L.; Wilkinson, Geoffrey. Basic Inorganic Chemistry, Third Edition. Wiley: New York 1995. pp597-608.

18. Greenwood, N. N., & Earnshaw, A. (2012). *Chemistry of the Elements*. Elsevier.

19. Crist, B. V. (2000). Handbook of monochromatic XPS spectra, The elements of native Oxides. *Handbook of Monochromatic XPS Spectra, The Elements of Native Oxides, by B. Vincent Crist, pp. 548. ISBN 0-471-49265-5. Wiley-VCH, October 2000.*, 548.

20. Toebes, M. L., van Dillen, J. A., & de Jong, K. P. (2001). Synthesis of supported palladium catalysts. *Journal of Molecular Catalysis A: Chemical, 173*(1-2), 75-98.

21. Miller, J. B., & Malatpure, M. (2015). Pd catalysts for total oxidation of methane: Support effects. *Applied Catalysis A: General, 495*, 54-62.

22. Chen, X., Schwank, J. W., Fisher, G. B., Cheng, Y., Jagner, M., McCabe, R. W., ... & Pan, X. (2014). Nature of the two-step temperature-programmed decomposition of PdO supported on alumina. *Applied Catalysis A: General, 475*, 420-426.

23. Schwartz, W. R., & Pfefferle, L. D. (2012). Combustion of methane over palladium-based catalysts: support interactions. *The Journal of Physical Chemistry C, 116*(15), 8571-8578.

24. Aluminum Oxide. Pubchem CID:9989226. https://pubchem.ncbi.nlm.nih.gov/compound/aluminum_oxide#section=Top

25. Aluminum Oxide. Toxnet CASRN: 1344-28-1. https://toxnet.nlm.nih.gov/cgi-bin/sis/search/a?dbs+hsdb:@term+@DOCNO+506

26. Goodman, E. D., Dai, S., Yang, A. C., Wrasman, C. J., Gallo, A., Bare, S. R., ... & Cargnello, M. (2017). Uniform Pt/Pd Bimetallic Nanocrystals Demonstrate Platinum Effect on Palladium Methane Combustion Activity and Stability. *ACS Catalysis, 7*(7), 4372-4380.

27. Persson, K., Thevenin, P. O., Jansson, K., Agrell, J., Järås, S. G., & Pettersson, L. J. (2003). Preparation of alumina-supported palladium catalysts for complete oxidation of methane. *Applied Catalysis A: General*, *249*(1), 165-174

28. Shirai, T., Watanabe, H., Fuji, M., & Takahashi, M. (2010). Structural properties and surface characteristics on aluminum oxide powders.

29. Bychkov, V. Y., Tulenin, Y. P., Slinko, M. M., Khudorozhkov, A. K., Bukhtiyarov, V. I., Sokolov, S., & Korchak, V. N. (2016). Self-oscillations during methane oxidation over Pd/Al2O3: Variations of Pd oxidation state and their effect on Pd catalytic activity. *Applied Catalysis A: General*, *522*, 40-44.

30. Ota, A., Kunkes, E. L., Kröhnert, J., Schmal, M., & Behrens, M. (2013). Particle size effect in methane activation over supported palladium nanoparticles. *Applied Catalysis A: General*, *452*, 203-213.

31. Samain, L., Jaworski, A., Edén, M., Ladd, D. M., Seo, D. K., Garcia-Garcia, F. J., & Häussermann, U. (2014). Structural analysis of highly porous γ-Al2O3. *Journal of solid state chemistry*, *217*, 1-8.

32. Chen, C., Cao, J., Cargnello, M., Fornasiero, P., & Gorte, R. J. (2013). High-temperature calcination improves the catalytic properties of alumina-supported Pd@ ceria prepared by self assembly. *Journal of catalysis*, *306*, 109-115.

33. Gremminger, A. T., de Carvalho, H. W. P., Popescu, R., Grunwaldt, J. D., & Deutschmann, O. (2015). Influence of gas composition on activity and durability of bimetallic Pd-Pt/Al2O3 catalysts for total oxidation of methane. *Catalysis Today*, *258*, 470-480

34. Ortloff, F., Bohnau, J., Graf, F., & Kolb, T. (2016). Removal of oxygen from (bio-) methane via catalytic oxidation of CH4—Reaction kinetics for very low O2: CH4 ratios. *Applied Catalysis B: Environmental*, *182*, 375-384

35. Sadokhina, N., Smedler, G., Nylén, U., Olofsson, M., & Olsson, L. (2017). The influence of gas composition on Pd-based catalyst activity in methane oxidation− inhibition and promotion by NO. *Applied Catalysis B: Environmental*, *200*, 351-360.

36. Sadokhina, N., Ghasempour, F., Auvray, X., Smedler, G., Nylén, U., Olofsson, M., & Olsson, L. (2017). An Experimental and Kinetic Modelling Study for Methane Oxidation over Pd-based Catalyst: Inhibition by Water. *Catalysis Letters*, *147*(9), 2360-2371.

37. Stefanov, P., Todorova, S., Naydenov, A., Tzaneva, B., Kolev, H., Atanasova, G., ... & Aleksieva, K. (2015). On the development of active and stable Pd–Co/γ-Al2O3 catalyst for complete oxidation of methane. *Chemical Engineering Journal*, *266*, 329-338.

38. Wagner, J. M. (2011). *X-ray photoelectron spectroscopy*. Nova Science Publishers.

39. Bozack, M. Auburn University. Personal Communication, 2017

40. Simplício, L. M. T., Brandão, S. T., Sales, E. A., Lietti, L., & Bozon-Verduraz, F. (2006). Methane combustion over PdO-alumina catalysts: The effect of palladium precursors. *Applied Catalysis B: Environmental*, *63*(1-2), 9-14.

41. Lin, J., Mei, T., Lv, M., Zhang, C. A., Zhao, Z., & Wang, X. (2014). Size-controlled PdO/graphene oxides and their reduction products with high catalytic activity. *RSC Advances*, *4*(56), 29563-29570.

42. Yoshida, H., Nakajima, T., Yazawa, Y., & Hattori, T. (2007). Support effect on methane combustion over palladium catalysts. *Applied Catalysis B: Environmental*, *71*(1-2), 70-79.

43. Kirkland, A. I., & Haigh, S. J. (Eds.). (2015). *Nanocharacterisation*. Royal Society of Chemistry.

44. Sulmonetti, T. Georgia Institute of Technology. Personal Communication. 2018

45. Ciuparu, D., Altman, E., & Pfefferle, L. (2001). Contributions of lattice oxygen in methane combustion over PdO-based catalysts. *Journal of Catalysis*, *203*(1), 64-74.

46. Narui, K., Yata, H., Furuta, K., Nishida, A., Kohtoku, Y., & Matsuzaki, T. (1999). Effects of addition of Pt to PdO/Al2O3 catalyst on catalytic activity for methane combustion and TEM observations of supported particles. *Applied Catalysis A: General*, *179*(1-2), 165-173.

47. Fujimoto, K. I., Ribeiro, F. H., Avalos-Borja, M., & Iglesia, E. (1998). Structure and reactivity of PdOx/ZrO2Catalysts for methane oxidation at low temperatures. *Journal of Catalysis*, *179*(2), 431-44

CATALYTIC OXIDATION OF METHANE OVER ALUMINA SUPPORTED PALLADIUM

OXIDES

A thesis submitted to the College of Letters and Science in partial fulfillment of the

requirements for the degree of

MASTER OF SCIENCE

DEPARTMENT OF CHEMISTRY

by

Jacqueline Michelle McGuire

2018

AcBanerju

Dr. Anil C. Banerjee

_03/15/2018_

Date

Zewdu Gebeyehu

Dr. Zewdu Gebeyehu

_03/15/2018_

Date

D. Wade Holley

Dr. D. Wade Holley

_3/15/2018_

Date